Alma Mater Studiorum · Università di Bologna

Scuola di Scienze
Dipartimento di Fisica e Astronomia
Corso di Laurea Magistrale in Fisica

Sleep-wake cycle: A new analysis for the two-step process model

Relatore:
Prof. Gastone Castellani

Correlatore:
Prof. Angelo Di Garbo

Presentata da:
Mattiangelo D'Agnese

Anno Accademico 2018/2019

Acknowledgements

I would like to thank my supervisor at the University of Bologna, Professor Gastone Castellani, who gave me the opportunity to work on this project. I also would like to thank Professor Angelo Di Garbo, my external supervisor, whose encouragements and useful critiques have been indispensable for the success of this research work. I am also deeply grateful to Dr. Francesco Sarnari, my tutor, mentor and friend, who helped me throughout the entire writing of this thesis. Last but not least, I would like to express my gratitude to Chiara Stirpe, for her patience and love during all these years and for her help and support in times of need. Without her this work would never have been possible.

Abstract

The sleep-wake cycle has been a subject of study for many applied scientists and mathematicians for more than thirty years. Nevertheless, there are still a lot of unanswered questions in this field. Understanding mechanisms and dynamics of the sleep-wake cycle is very important because its alterations can produce significant consequences on human health.

In this work we introduce a biologically-based mathematical model of the human sleep-wake cycle. The main novelty, compared to previous models, is the introduction of an accurate neuronal model, namely the Hodgkin-Huxley model, which allows us to describe the system by using more realistic synaptic connections.

We strongly believe that this topic merits a deep investigation, not only because of its physical and mathematical content, but also because of its potential impact on improving human health research.

Sommario

Il ciclo sonno-veglia è oggetto di studio per molti scienziati e matematici da più di trent'anni ma nonostante ciò molti quesiti non trovano ancora una risposta. Capire i meccanismi e le dinamiche del ciclo sonno-veglia è un problema molto importante perché le sue alterazioni possono avere conseguenze significative sulla salute umana.

In questo lavoro viene presentato un modello matematico, con basi biologiche, del ciclo sonno-veglia. La principale novità rispetto ai modelli precedenti è l'utilizzo di un accurato modello neuronale, il modello di Hodgkin-Huxley, che permette di descrivere il sistema usando connessioni sinaptiche realistiche.

Crediamo fermamente che questo argomento meriti una investigazione dettagliata, non solo per il contenuto fisico e matematico, ma anche per il suo potenziale impatto sulla ricerca nel campo della sanità.

Indice

Capitolo 1

Introduction

The mechanisms underpinning the sleep-wake cycle, such as the relation between the time spent awake and the timing of sleep or the biological interactions among the different cerebral areas, are still poorly understood, despite a century-old work. In order to cover this lack of knowledge, many experimental [22] and theoretical [11] studies have been performed. For example the main cerebral areas related to wake and sleep are known [21], however there are many unanswered questions, such as their precise role and the detailed functions performed by each area.

Understanding mechanisms and dynamics of the sleep-wake cycle is very important because its alterations can produce a significant impact on human health. Recent studies have shown a close relation between sleep disorders and other diseases [23, 25, 33]. Previous studies have also covered many aspects in investigating sleep processes, from chemical, to biological, to physiological and beyond [24, 26].

There are many physiological ingredients affecting the sleep-wake cycle, such as thermoregulation, hormonal dynamics and the eventual action of drugs, along with the effects of sleep deprivation. This renders very complicated building up a mathematical model which would take into account all possible variables.

Mathematical models able to capture several features of the sleep-wake cycle have been developed since middle-seventies, starting with the pioneering work by McCarley and Hobson [18], but the most important work in this field is probably the two-process model introduced by Borbély in the early eighties [4], which has been used as a reference for sequent mathematical models [5]: in his article the existence of two interacting oscillators is postulated, namely the homeostatic process (S) and the circadian process (C). S is related to the time spent awake while C is related the activity of the suprachiasmatic nucleus (SCN) which plays the role of pacemaker.

Another important step for this kind of models is represented by the paper by Phillips and Robinson [19], in which the interaction between the ventrolateral preoptic area (VLPO) and the monoaminergic nuclei (AMIN) is considered, in a mean field appro-

ximation. Under these assumptions they have built a biologically-based mathematical model able to reproduce several features of the sleep-wake cycle.

Subsequently, Rempe et al. [1] develop a mathematical model using a Morris-Lecar-like neuron model (where the Morris-Lecar system [10] is a bi-dimensional reduction of the Hodgkin-Huxley neuron model [3]) in order to represent the different cerebral areas, while in previous studies [[]] the mean field approximation were performed through ad-hoc equations using physiology parameters.

Our work is based on this latter model. The main contribution consists in replacing of the Morris-Lecar-like neurons with Hodgkin-Huxley neurons, which is more complete and accurate neuronal model. Since previous approaches are mostly based on heuristic simplified models, which result in being quite distant from the description of the underlying physiology, our aim is to show that it is possible to develop a mathematical model able to capture several features of the human sleep-wake cycle using an accurate neuronal model to represent cerebral areas.

There are, of course, many limitations in this model, for example some cerebral regions, which may play an important role in the cycle, have been neglected, in order to study reduced model. In addiction, the assumption to reach the mean field approximation using a single neuron is a strong simplification, in fact the nervous system is extremely complex and it is composed by billions of interacting neurons. Anyway this kind of model is considerably different from the already existing ones and it could open a new line of research in this field.

Capitolo 2

Structure of nervous system

The nervous system is composed of a huge number of cells, called neurons, in tight connection with each other through links called synapses.

In this chapter a brief description of neurons and synapses, from a biological point of view, is presented[1]. Their description in terms of mathematical models will be provided in the next chapters.

2.1 Neurons

The nervous system is composed of more than 100 billions of neurons. Neurons are cells whose function is to receive and transmit information through electric signals.

Its structure is represented in figure (2.1): a cell body or **soma**, which contains the cellular nucleus and other organelles; the **dendrites**, which are branched fibre extensions that propagate the electrochemical stimulation received from neighbouring cells to the soma; the **axon**, which is a long and slender projection of the neuron, whose function is to conduct information as electric impulses or **action potentials** to other neurons, muscles or glands.

The dendrites in a neuron can be hundreds or even thousands and may be branched themselves to receive signals from other thousands of cells, so that the neural network composing the nervous system is deeply connected and extremely complex. The axon is surrounded by a **myelin sheath**, a fatty tissue, which acts as an insulator and allows faster transmission of electric impulses until the axon ends, called **terminal buttons**.

The nervous system works via electrochemical processes. Electrical charged chemicals move across the neuron itself and transmit information between neighbouring neurons. The electric signal is received by the dendrites, transmitted to the soma and, if a threshold is exceeded, passes on to the axon until the terminal buttons which emit chemicals, called **neurotransmitters**, to other neurons through the synapses.

[1] A more complete description can be found in virtually any neuroscience book, for example [20]

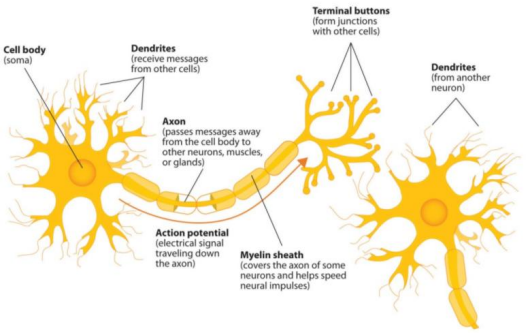

Figura 2.1: Structure of a typical neuron [27].

Every cell has an electric potential difference between its inside and outside, called **membrane potential**. Typical values float around -70 mV. In stationary conditions the potential is called **resting potential**, which can be calculated using the Nernst equation and the Goldman-Hodgkin-Katz equation[2].

As we said before, if the signal is strong enough, namely if the electric current exceeds a threshold, the neuron start firing. This means the membrane potential varies with time through one or more spikes, the action potentials, and the signal is transmitted to the other cells. A single spike of action potential typically lasts 1 or 2 ms and the difference of potential between its maximum and minimum values is about 100 mV. After this, if the current comes back under the threshold, the cell returns to its resting potential. Note that the action potential operates in such a way that either the neuron fires completely or it does not fire at all.

As a conclusion of this paragraph, we state that the transmission of the action potentials across the axon, even though there are several complications [8], is described by the Cable equation:

$$C\frac{\partial V}{\partial t} = \frac{a}{2r}\frac{\partial^2 V}{\partial x^2} - I(x,t), \tag{2.1}$$

where a is the radius of the cylindrical cable, r is its resistance, V is the membrane potential, I is the current and C is the membrane capacitance. Such a kind of equations, called partial differential equations (PDEs), can be studied using the techniques of dynamical systems and bifurcation theory, which will be developed in next chapter. However, we will focus only on ordinary differential equations (ODEs) but the discussion can be generalized to PDEs.

[2]See for example [8] for further details.

2.2 Synapses

The junctions areas between the terminal buttons at the end of the axon of a neuron and the dendrites of another neuron are called synapses. Through these regions the transmission of information occurs, thus neighbouring neurons can communicate. Mainly there exist two kind of synapses: **chemical** and **electical**. We begin by describing the former.

In a chemical synapse the communication between two neurons is conveyed by the release of chemicals, the neurotransmitters, from the presynaptic neuron to the postsynaptic neuron. This situation happens when the action potential reaches the end of the axon and the neurotransmitters are released through vesicles. The vesicles containing the neurotransmitter leave the terminal buttons and are collected by the relative receptors in the dendrites of the next neuron.

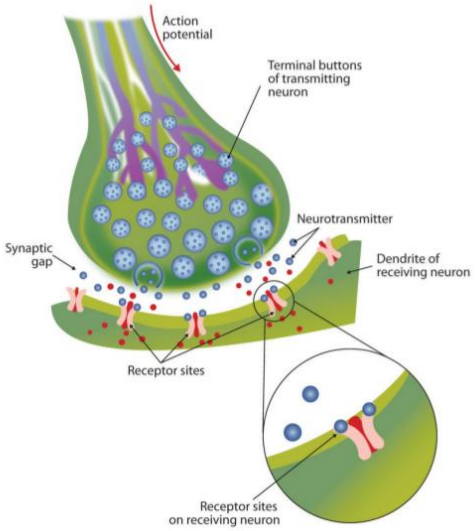

Figura 2.2: A chemical synapse between two neighbouring neurons [27].

The neurotransmitters, depending on their nature, may be excitatory or inhibitory. If the entering current reaches the threshold, another action potential is generated by the cell and the process can continue.

Not every neuron accepts every neurotransmitter, in fact each receptor allows entrance of a particular kind of chemical. Those which do not enter through the receptors are removed out of the synapse by particular enzymes and reabsorbed into the terminal buttons.

Substances similar to the neurotransmitters, called **agonists**, may be collected by the receptors instead of the original neurotransmitters and perturb the transmission mechanisms. An example is represented by cocaine which is an agonist of dopamine,

a neurotransmitter that produces feelings of pleasure when released by neurons, thus cocaine creates similar effect when ingested.

On the other hand, there is another class of chemicals, the **antagonists**, which inhibits the effects of a neurotransmitter. Their action is to bind to the receptor sites of dendrites and block absorption. As an example, consider the poison curare which is an antagonist for the neurotransmitter acetylcholine. When this poison enters the neurons, it stops the connections among them and may cause death.

These kind of perturbations may affect many mechanisms of communication in the nervous system and their behaviour under normal conditions, including the sleep-wake cycle.

In contrast to chemical synapses, electrical synapses allows a direct flux of electric charges between neurons through particular narrow channels, the **gap-junctions**. Due to the fact that this kind of synapse does not require vesicles, the transmission of impulses is much faster than in chemical synapses. For this reason, electrical synapses can be found in cerebral areas where a rapid response is needed, for example in those related to defensive reflexes. Also note the transmission can be inwards and outwards, while in chemical synapses it is one way.

2.3 Ionic channels

In section (2.1) we mentioned the membrane potential, here we explain in deeper detail its nature.

As we already said, the membrane potential is defined by the difference of potential between inside and outside of the cell:

$$V_M = V_{in} - V_{out}, \tag{2.2}$$

and, at resting potential, this value is about -70 mV. Changes in V_M are due to incoming and outcoming electric currents via the **ionic channels**, which are narrow gates that allow electric charges to move across the cell membrane. The main electric charges are Na^+, K^+ and Cl^- ions: their concentrations inside and outside the cell determine the membrane potential.

Ionic channels are divided into two classes: gated and non-gated. Each ion has its related gated ionic channel, which allows the passage of only that particular ion , while non-gated channel are always open and ions flow across the membrane by passive diffusion. Gated channels are voltage-dependent, which means the probability of a gate to be open depends mainly on the membrane potential. Typically non-gated channels are responsible for resting potential and opening and closure of gated channels are associated with action potentials. If the concentration of ions is the same both inside and outside the cell, then the system is in equilibrium and the resting potential can be computed

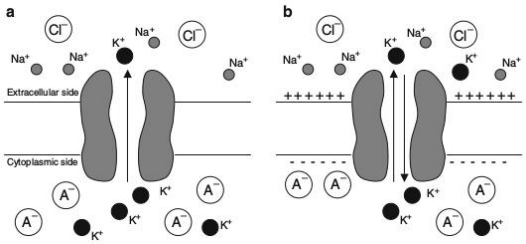

Figura 2.3: A schemata of K^+ gated ionic channel. (a) If the concentration of potassium is greater inside than outside the cell then K^+ ions more probably will flow outwards. (b) If the concentration is the same in both sides there is no net flux of ions [8].

using the Nernst equation or its generalization, the Goldman-Hodgkin-Katz equation:

$$V_M = \frac{RT}{F} \frac{\sum_j P_j [j]_{out}}{\sum_j P_j [j]_{in}}, \tag{2.3}$$

where R is the ideal gas constant, T the temperature, F the Faraday's constant, P_j the permeability of j-th ion and $[j]$ the concentration [8].

We conclude this chapter stating that, due to the fact that the cell activity is connected to its electric properties, the cell membrane is modelled as an electric circuit. For example the Hodgkin-Huxley model is based on the circuit in figure (2.4).

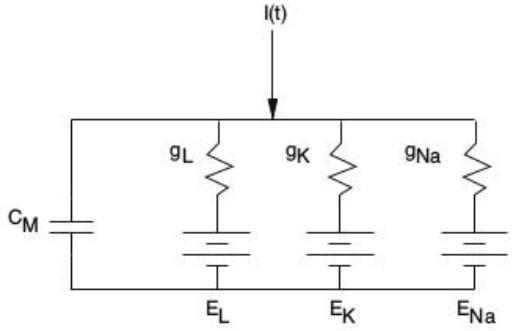

Figura 2.4: Equivalent circuit underlying the Hodgkin-Huxley model [8].

The next chapter is dedicated to outline the main concepts of dynamical systems and bifurcation theory, in order to finally introduce neurons from a mathematical point of view.

Capitolo 3

Dynamical systems and bifurcation theory

This chapter deals with a short introduction to bifurcation theory in dynamical systems. After that a definition of dynamical systems is given, the analysis of linear stability of fixed points in 1-dimensional and 2-dimensional systems is discussed, then a classification of the main bifurcations is presented. The main advantage in studying low-dimensional systems is the possibility to have a direct geometric intuition, as we will see. In high-dimensional systems the bifurcations introduced in the next paragraphs are still valid and new ones can occur, but we will limit our discussion to 1 and 2 dimensions.

3.1 Introductory definitions

3.1.1 Dynamical systems

A very informal definition of a **dynamical system** is the following: it is a mathematical formalization of the concept of a deterministic process. A state in the future or in the past of many physical, chemical, biological, etc systems may be inferred by knowing the present state and the laws governing the evolution. If these laws do not change in time, then the behaviour of the system is completely determined by its initial conditions. In conclusion, a dynamical system is defined by a set of possible states and the law which settles the evolution of the states in time [28].

More precisely, a dynamical system is defined by a triple $\{T, X, \varphi^t\}$, where T is a number set, X is a state space and φ^t is an evolution operator. Typically $t \in T$ is identified as the time: in discrete-time dynamical systems $T \in \mathbf{Z}$, in continuous-time dynamical systems $T \in \mathbf{R}$. The possible states in state space are identified by the points in a set X. Finally, the evolution operator φ^t is defined for every $t \in T$ as:

$$\varphi^t : X \to X, \tag{3.1}$$

and transforms an initial state $x_0 \in X$ in a state $x_t \in X$ at time t as:

$$x_t = \varphi^t x_0. \tag{3.2}$$

In addiction, the evolution operator has to satisfy the two following properties:

$$x_0 = \varphi^0 x_0, \tag{3.3}$$

which means that φ^0 is the identity operator and:

$$x_{t+s} = \varphi^{t+s} x_0 = \varphi^t(\varphi^s x_0), \tag{3.4}$$

which means that the final state x_{t+s} is the same if the system evolves for a time $t+s$ or if it evolves for a time s and then for a time t.

For our purposes we limit our discussion to continuous-time dynamical systems, thus $T \in \mathbf{R}$, in a state space $X \in \mathbf{R}^n$ and the evolution operator is defined by ordinary differential equations. From now on we use the terms *dynamical system* and *ordinary differential equation* as synonyms.

3.1.2 Bifurcations

If a dynamical system depends on one or more parameters, it can happen that varying these parameters, the qualitative behaviour of the system can change, for example fixed points can be created or destroyed, their stability can change, even periodic solutions arise. These kind of changes are called **bifurcations**.

In the following we will refer to well-behaved real-valued functions, in the sense they are sufficiently smooth and allows all the derivatives we will need.

3.2 Fixed points and stability in 1 dimension

We begin our discussion on fixed points by considering the ODE:

$$\dot{x} = f(x), \tag{3.5}$$

where D is a subset of $\mathcal{R}$, $f : D \to \mathcal{R}$ is a smooth function and $x \in D$, then a **fixed point** x^* is defined by:

$$f(x^*) = 0, \tag{3.6}$$

namely it is an equilibrium solution of (3.5):

$$x(t) = x^*. \tag{3.7}$$

Note that (3.5) has an exact general solution obtained by separation of variables:

$$t = t_0 + \int_{x_0}^{x} \frac{dx'}{f(x')}. \tag{3.8}$$

We now focus our attention on the stability of equation (3.7), roughly speaking we are asking ourselves: *"what happens to equilibrium solutions after a perturbation?"*.

In order to answer this question we apply a procedure called **linearization**, thus we define a small deviation $\eta(t) = x(t) - x^* \ll 1$ and check its behaviour:

$$\dot{\eta} = \dot{x} = f(x^* + \eta) \simeq f(x^*) + f'(x^*)\eta = f'(x^*)\eta, \tag{3.9}$$

where we neglected the quadratic term in η and supposed $f'(x^*) \neq 0$. If this is the case[1] then (3.9) has the solution:

$$\eta(t) = \eta(0)e^{f'(x^*)t}, \tag{3.10}$$

which means $\eta(t)$ decays if $f'(x^*) < 0$ (x^* is **stable**) or grows if $f'(x^*) > 0$ (x^* is **unstable**).

3.3 Fixed points and stability in 2 dimensions

Consider the system of coupled ODEs:

$$\dot{\vec{X}} = \vec{F}(\vec{X}), \tag{3.11}$$

where U is a subset of $\mathcal{R}^2$, $\vec{F} : U \to \mathcal{R}^2$ is a smooth vector field defined as $\vec{F}(\vec{X}) = (f(\vec{X}), g(\vec{X}))^T$, $\vec{X} = (x, y) \in U$. Supposing (x^*, y^*) is a fixed point:

$$f(x^*, y^*) = g(x^*, y^*) = 0, \tag{3.12}$$

then:

$$u = x - x^* \ll 1, \tag{3.13}$$
$$v = y - y^* \ll 1, \tag{3.14}$$

define a small deviation from the fixed point and its dynamics is given by:

$$\begin{aligned} \dot{u} = \dot{x} = f(x^* + u, y^* + v) \simeq \\ f(x^*, y^*) + u\partial_x f(x^*, y^*) + v\partial_y f(x^*, y^*) = \\ = u\partial_x f(x^*, y^*) + v\partial_y f(x^*, y^*), \end{aligned} \tag{3.15}$$

[1] If $f'(x^*) = 0$ nothing can be said about stability and the problem has to be studied case by case.

and similarly:

$$\dot{v} = u\partial_x g(x^*, y^*) + v\partial_y g(x^*, y^*), \tag{3.16}$$

in which quadratic terms in u and v are neglected. In this case the deviation evolves according to the **linearized system** (until quadratic terms are negligible) which can be solved exactly:

$$(\dot{u}, \dot{v})^T = J(x^*, y^*)(u, v)^T, \tag{3.17}$$

where $J(x^*, y^*)$ is the Jacobian matrix at the fixed point.

Since we are interested in studying the stability we only care about the behaviour of the system close to fixed points, thus linearization is a good approximation[2]. Due to the fact $J(x^*, y^*)$ is a symmetric matrix, it can always be rewritten in terms of eigenvalues and eigenvectors. The general solution of a generic 2-dimensional linear system of ODEs:

$$\dot{\vec{x}} = A\vec{x}, \tag{3.18}$$

is given by:

$$\vec{x}(t) = c_1 e^{\lambda_1 t}\vec{w}_1 + c_2 e^{\lambda_2 t}\vec{w}_2, \tag{3.19}$$

where λ_i is the eigenvalue associated to the eigenvector $\vec{w}_i$, $i = 1, 2$ of matrix A.

In order to check the stability of the fixed point (x^*, y^*), it is sufficient to look at the sign of the real part of the eigenvalues: if at least one of them is positive, then (3.19) grows exponentially and the fixed point is unstable. On the other hand, if the real parts are all negative then the fixed point is stable. Imaginary parts do not affect the global stability, even though have impact on the trajectories: for example a stable fixed point is a node if $Im(\lambda_{1,2}) = 0$, but it is a spiral if $Im(\lambda_{1,2}) \neq 0$.

An additional tool, which allows us to find fixed points graphically, is represented by the study of **nullclines**. A nullcline is defined as the curve on which the time derivative of a variable in the dynamical system is equal to zero, namely, for equation (3.11), the nullclines are the curves defined by $f(x, y) = 0$ and $g(x, y) = 0$, which can be plotted on phase plane. By definition, the points at which these curves cross are fixed points.

The definitions we introduced in order to study stability or instability of fixed points are pretty general and valid even for higher-dimensional systems.

3.4 Limit cycles

The dynamics in 1 dimension is pretty poor, in fact a trajectory in phase space can only approach, be repelled or stand on a fixed point. In 2 dimensions oscillations and periodic orbit can arise, in addiction to the already-known behaviour seen in 1 dimension.

[2]Actually particular cases in which this approximation is not enough exist but we do not investigate further.

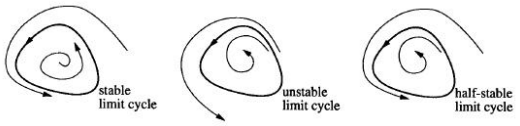

Figura 3.1: The three kinds of limit cycles [7].

A **limit cycle** is an isolated closed trajectory, which means that neighboring trajectories are not closed: they approach the limit cycle (if the limit cycle is stable) or move away from it (if the limit cycle is unstable). There also exist half-stable limit cycles: trajectories are attracted on one side and repelled on the other.

Note that limit cycles occur only in nonlinear systems. In linear systems of course closed orbits are possible but they are not isolated: if $\vec{x}(t)$ is a closed orbit, because of linearity also $c\vec{x}(t)$ does, which means $\vec{x}(t)$ is surrounded by a one-parameter family of closed orbits.

3.5 Bifurcations in 1 dimension

In this section the main bifurcations in 1 dimension, which occur also in higher dimensional systems, are outlined and a few examples are provided.

3.5.1 Saddle-node bifurcation

The saddle-node bifurcation is the mechanism that manages the creation and destruction of fixed points. As control parameter is varied, two fixed points can move closer to each other, collide and mutually annihilate at bifurcation point.

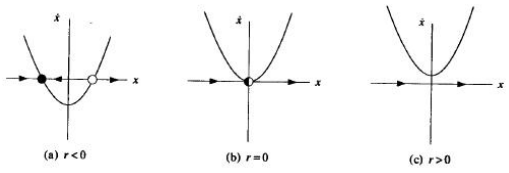

Figura 3.2: Saddle-node bifurcation [7].

The normal form of this kind of bifurcation is given by:

$$\dot{x} = r + x^2, \tag{3.20}$$

where r is the control parameter.

As shown in figure (3.2), the two fixed points $x^* = \pm\sqrt{-r}$, one stable and the other unstable, exist if $r < 0$ and approach or move away each other as r varies. If $r < 0$ is

increased the fixed points come closer and in $r = 0$ they collide and disappear. On the other hand if $r > 0$ is decreased two fixed points emerge in $r = 0$ and then move away. In $r = 0$ the system changes its qualitative behaviour so this is the bifurcation point.

In order to represent this situation we can plot the **bifurcation diagram** which shows the dependence of fixed points as a function of r, as shown in figure (3.3).

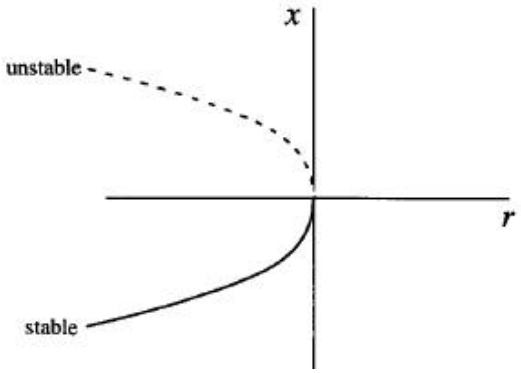

Figura 3.3: Saddle-node bifurcation diagram [7].

3.5.2 Transcritical bifurcation

The transcritical bifurcation manages the exchange of stabilities between two fixed point after they collided. This kind of bifurcation typically occurs when a fixed point always exists and cannot be destroyed.

The normal form of this kind of bifurcation is given by:

$$\dot{x} = rx - x^2. \tag{3.21}$$

In this case the fixed points are $x^* = 0$ and $x^* = r$.

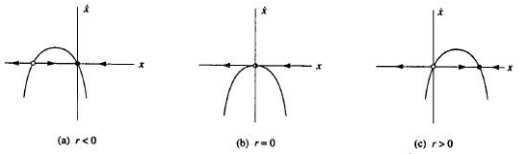

Figura 3.4: Transcritical bifurcation [7].

As shown in figure (3.4), $x^* = 0$ is a fixed point for all values of r and, if $r < 0$, it is stable and $x^* = r$ is unstable. On the other hand if $r > 0$ then $x^* = 0$ becomes unstable and $x^* = r$ becomes stable. This means the two fixed points at bifurcation point $r = 0$ exchange their stability, as also shown in the bifurcation diagram in figure (3.5).

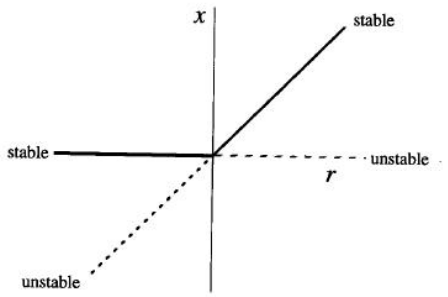

Figura 3.5: Transcritical bifurcation diagram [7].

3.5.3 Pitchfork bifurcation

The pitchfork bifurcation occurs in systems presenting some kind of symmetry and so fixed points tend to appear and disappear is symmetrical pairs. There exist two kind of pitchfork bifurcation: **supercritical** and **subcritical**.

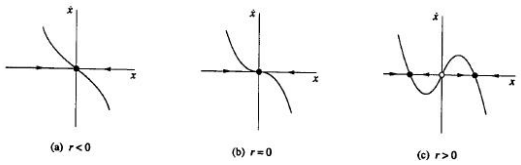

Figura 3.6: Supercritical pitchfork bifurcation [7].

The normal form of the **supercritical** pitchfork bifurcation is given by:

$$\dot{x} = rx - x^3, \tag{3.22}$$

whose fixed points are $x^* = 0$ and, if $r > 0$, $x^* = \pm\sqrt{r}$.

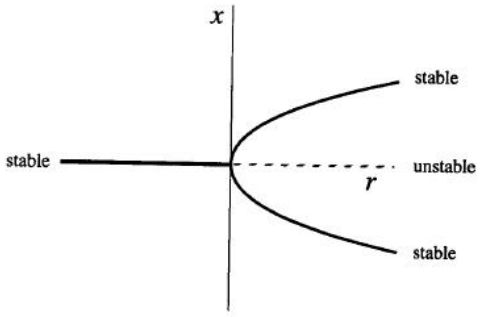

Figura 3.7: Supercritical pitchfork bifurcation diagram [7].

As shown in figure (3.6), $x^* = 0$ is the only existing fixed point if $r \leq 0$ and it is stable. If $r > 0$ then it becomes unstable and the two symmetrical stable fixed points $x^* = \pm\sqrt{r}$ appear, so $r = 0$ is the bifurcation point, as also shown in the bifurcation diagram in figure (3.7). The reasons of the name "pitchfork" now should be clear!

The normal form of the **subcritical** pitchfork bifurcation is:

$$\dot{x} = rx + x^3. \tag{3.23}$$

As in the previous case, $x^* = 0$ always exists but now is stable if $r < 0$ and $x^* = \pm\sqrt{-r}$ are unstable. Conversely, if $r \geq 0$ then $x^* = 0$ is the only fixed point and it is unstable, as shown in figure (3.8).

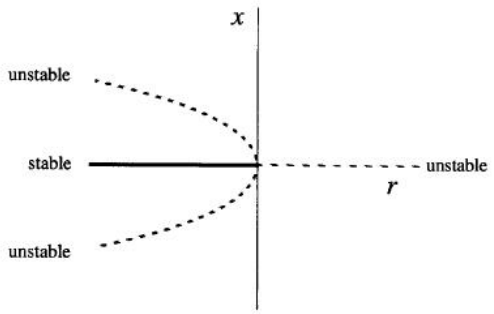

Figura 3.8: Subcritical pitchfork bifurcation diagram [7].

3.6 Bifurcations in 2 dimensions

The dynamics in 2 dimensions is richer than in 1 dimension. In addiction to the bifurcations seen in the previous sections, in fact, new kinds of bifurcations involving limit cycles may arise.

3.6.1 Hopf bifurcation

Given a fixed point, as said in section 3.3, its stability is regulated by the real part of the eigenvalues λ_1, λ_2 of the Jacobian matrix. Since they satisfy a quadratic equation, if the fixed point is stable, they must be real and negative or complex conjugates with negative real part (see figure (3.9)).

In order to destabilize the fixed point, at least one of the two eigenvalues has to cross the imaginary axis, as the control parameter μ varies. If both complex conjugates eigenvalues do, the system undergoes an Hopf bifurcation.

A **supercritical** Hopf bifurcation occurs when a stable fixed point becomes unstable and is surrounded by a small limit cycle.

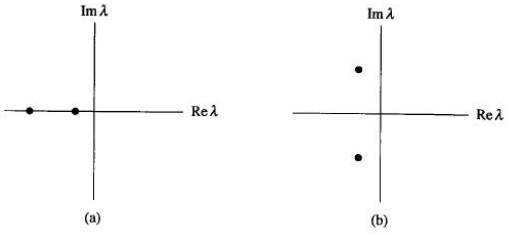

Figura 3.9: Jacobian eigenvalues of a stable fixed point in complex plane. (a) Both real. (b) Complex conjugates [7].

The normal form in polar coordinates is given by:

$$\begin{aligned} \dot{r} &= \mu r - r^3, \\ \dot{\theta} &= \omega. \end{aligned} \tag{3.24}$$

After a computation, the eigenvalues of the Jacobian are found to be $\lambda = \mu \pm i\omega$, so the bifurcation point is $\mu_c = 0$. As shown in figure (3.10) the origin $r = 0$ is stable if $\mu \leq 0$. If $\mu > 0$ it becomes unstable and a stable circular limit cycle of radius $r = \sqrt{\mu}$ appears.

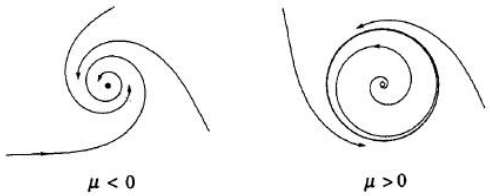

Figura 3.10: Phase plane in supercritical Hopf bifurcation [7].

It can be shown that, in general in supercritical Hopf bifurcation, the size of the limit cycle grows continuously from zero of a factor proportional to $\sqrt{\mu - \mu_c}$ and the period of the limit cycle is $T = 2\pi/Im(\lambda) + O(\mu - \mu_c)$, for $\mu - \mu_c$ close to zero.

In **subcritical** Hopf bifurcation the trajectories jump to a distant attractor (a fixed point, a limit cycle, infinity). This means there is not a continuous growth of a limit cycle as in the supercritical case.

The normal form is given by:

$$\begin{aligned} \dot{r} &= \mu r + r^3 - r^5, \\ \dot{\theta} &= \omega. \end{aligned} \tag{3.25}$$

Note that r^3 is now the destabilizing term.

If $\mu < 0$, there is a stable fixed point in the origin surrounded by an unstable limit cycle and an external stable limit cycle. As μ increases, the unstable limit cycle shrinks

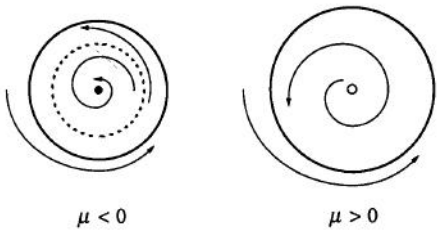

Figura 3.11: Phase plane in subcritical Hopf bifurcation [7].

to zero amplitude and makes the origin become unstable at the bifurcation point $\mu = 0$. This means that there is a trajectory rapidly emerging from the origin which approaches the stable limit cycle after the bifurcation.

3.6.2 Saddle-node bifurcation of cycles

Consider once again equation (3.25): we have seen in previous section if $\mu = 0$ a subcritical Hopf bifurcation occurs, anyway another kind of bifurcation may occur too.

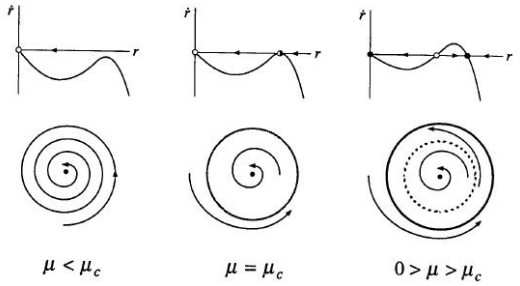

Figura 3.12: Radial plot and phase plane in saddle-node bifurcation of cycles [7].

As shown in figure (3.12), if $\mu_c = -1/4$, an half-stable limit cycle appears and, as μ is increased, it splits into two limit cycles, in a sort of saddle-node bifurcation. This kind of bifurcation is called **saddle-node bifurcation of cycles**.

3.6.3 Saddle-node on a limit cycle (SNLC) bifurcation

The **SNLC** bifurcation occurs when two fixed points emerge on a limit cycle in a saddle-node bifurcation.

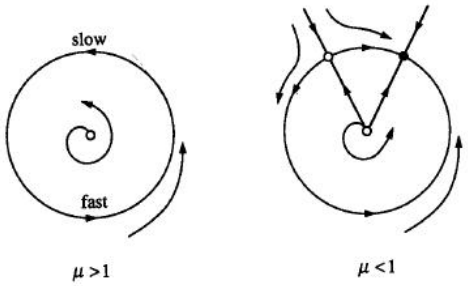

Figura 3.13: Phase plane in SNLC bifurcation [7].

As an example we consider[3]:

$$\begin{aligned} \dot{r} &= r - r^3, \\ \dot{\theta} &= \mu - sin(\theta). \end{aligned} \tag{3.26}$$

As shown in figure (3.13), if $\mu > 1$, the trajectories approach the stable limit cycle $r = 1$ surrounding the origin which is always unstable. As μ decreases, a bottleneck appears at $\theta = \pi/2$ and finally, at bifurcation point $\mu_c = 1$, a fixed point emerges on the limit cycle and the period becomes infinite (it can be shown the period is $T = O(1/\sqrt{\mu - \mu_c})$ near the bifurcation). If $\mu < 1$ the fixed point splits into a saddle and node in a saddle-node bifurcation.

3.6.4 Saddle-homoclinic bifurcation

A **saddle-homoclinic** bifurcation occurs when a limit cycle and a saddle move closer until they touch at bifurcation point, thus making the orbit homoclinic.

As an example consider:

$$\begin{aligned} \dot{x} &= y, \\ \dot{y} &= \mu y + x - x^2 + xy. \end{aligned} \tag{3.27}$$

In figure (3.14) the phase plane is plotted for different values of μ: if $\mu < \mu_c \simeq -0.8645$, a stable limit cycle surrounds the unstable fixed point on the right and there is a saddle at the origin. As μ increases, the limit cycle moves closer to the saddle until $\mu = \mu_c$, where they touch, and the orbit becomes homoclinic. Finally, if $\mu > \mu_c$, the limit cycle is destroyed.

We conclude this paragraph noting that also in this case the period becomes infinite but the asymptotic behaviour is different than in SNLC bifurcation: $T = O(\ln(\frac{1}{\mu - \mu_c}))$ near the bifurcation point.

[3] $\dot{\theta}$ equation is known as Adler's equation.

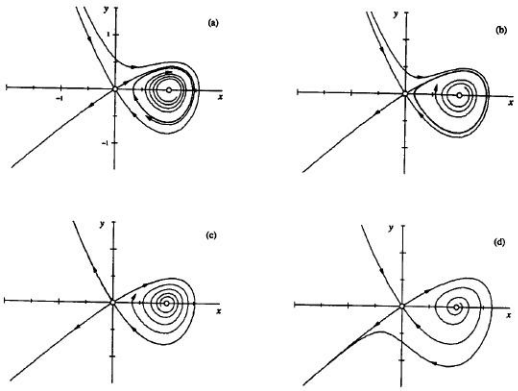

Figura 3.14: Phase plane in saddle-homoclinic bifurcation for different values of μ [7].

In the next chapters the Morris-Lecar model and the Hodgkin-Huxley model are studied. These neuronal models could be seen as two additional examples of bifurcations in dynamical system and then they could be presented together in this chapter. However, due to their relevance, we prefer to discuss them in separate chapters.

Capitolo 4

Morris-Lecar model

Morris-Lecar model [10] is a neuronal model described by two coupled nonlinear ODEs and several kinds of bifurcations may occur. Its importance is due to the fact that, despite its simplicity, it presents the typical feature of neurons, namely it fires if an external current is applied.

The model is defined by the following coupled equations:

$$\begin{aligned} C_M\dot{V} &= I_{app} - g_L(V - E_L) - g_K n(V - E_K) - g_{Ca} m_\infty(V)(V - E_{Ca}), \\ \dot{n} &= \frac{\Phi(n_\infty(V) - n)}{\tau_n(V)}, \end{aligned} \tag{4.1}$$

where:

$$m_\infty(V) = \frac{1 + \tanh(\frac{V - V_1}{V_2})}{2}, \tag{4.2}$$

$$n_\infty(V) = \frac{1 + \tanh(\frac{V - V_3}{V_4})}{2}, \tag{4.3}$$

$$\tau_n(V) = 1/\cosh\left(\frac{V - V_3}{2V_4}\right), \tag{4.4}$$

and I_{app} is the control parameter.

Depending on the choice of the parameters a particular bifurcation occurs. Three different sets of parameters are recorded in table (4.1) and are studied in next sections.

4.1 Hopf bifurcation

Here the parameters are chosen as in the Hopf column in table (4.1). In figure (4.1) there is a plot of the bifurcation diagram. A unique fixed point is present for each value of I_{app}, represented by the central curve. The other two branches represent the maximum and

Parameter	Hopf	SNLC	Homoclinic
Φ	0.04	0.067	0.23
g_{Ca}	4.4	4	4
V_3	2	12	12
V_4	30	17.4	17.4
E_{Ca}	120	120	120
E_K	-84	-84	-84
E_L	-60	-60	-60
g_K	8	8	8
g_L	2	2	2
V_1	-1.2	-1.2	-1.2
V_2	18	18	18
C_M	20	20	20

Tabella 4.1: Morris-Lecar parameters. $V_1, V_2, V_3, V_4, E_{Ca}, E_K, E_L$ are expressed in mV, g_{Ca}, g_K, g_L in mS/cm^2, C_M in $\mu F/cm^2$, I_{app} in $\mu A/cm^2$ and ϕ is adimensional.

minimum amplitude of the limit cycle. Blue parts represent stable behaviours while red parts mean instability. The existence of just one fixed point can be understood looking at figures (4.4(a)) and (4.4(b)): the nullclines intersect only once.

In $I_{app} = 94$ and $I_{app} = 212$ the fixed point changes its stability and a subcritical Hopf bifurcation occurs, as also suggested by the finite frequency of the orbit at bifurcations, as shown in figure (4.3). Note also there are two tiny overlaps in $88.3 < I_{app} < 94$ and $212 < I_{app} < 217$, where the system is bistable: the fixed point is stable and the stable limit cycle also exists. In these two intervals the fixed point is surrounded by an unstable limit cycle (not shown in the figures) which emerges in $I_{app} = 88.3$ and $I_{app} = 217$: here a saddle-node bifurcation of cycles occurs.

Several numerical solutions, as examples, and a plot of the eigenvalues at the fixed point as the applied current varies, are shown below. This latter kind of plots is very useful in order to determine the nature of fixed points.

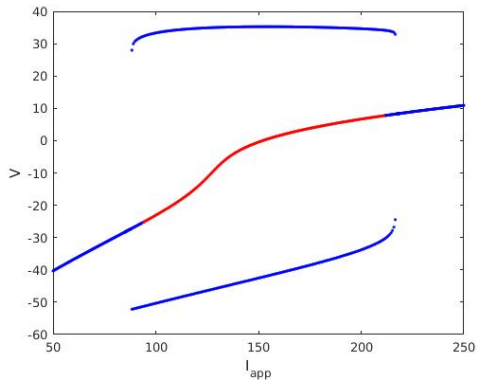

Figura 4.1: Bifurcation diagram in Hopf bifurcation parameters choice: voltage as a function of applied current. Blue branches are stable and red branches are unstable.

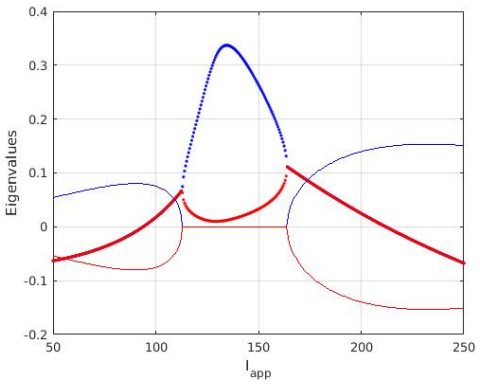

Figura 4.2: Eigenvalues of the jacobian matrix at the fixed point as functions of current. Thick and dashed lines correspond to the real parts, fine and continuous lines correspond to the imaginary parts. Note that real parts are positive in the range $94 < I_{app} < 212$, hence the fixed point is unstable, otherwise it is stable.

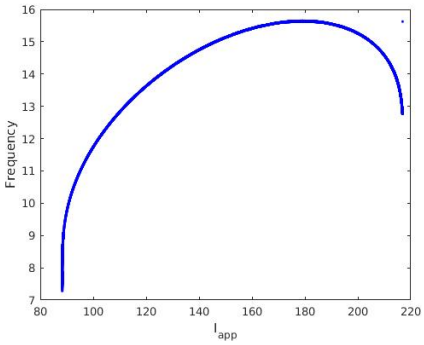

Figura 4.3: Frequency (Hz) as a function of current for stable limit cycles. The sudden appearing and disappearing of finite-frequency limit cycles suggest a saddle-node bifurcation of cycles.

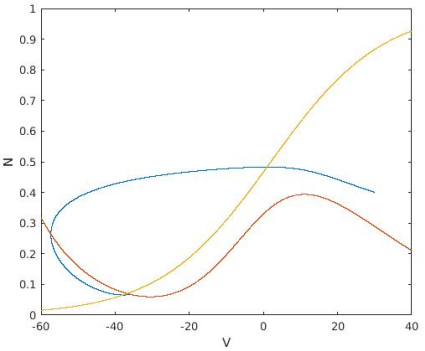

((a)) $I_{app} = 60$ and the orbit approaches the stable fixed point.

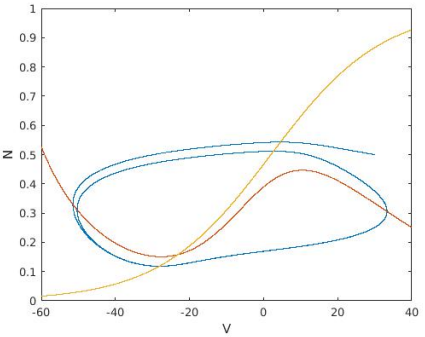

((b)) $I_{app} = 100$, the fixed point is unstable and the orbit approaches the stable limit cycle.

Figura 4.4: Orbits in phase plane with nullclines. Blue curves are the orbits, yellow curves are N-nullclines and red curves are V-nullclines.

4.2 SNLC bifurcation

Choosing the parameters as in SNLC column in table (4.1) a SNLC bifurcation occurs. Looking at figure (4.5), the bifurcation diagram, we can see there is only a stable fixed point if $I_{app} < -10$, then in the range $-10 < I_{app} < 40$ the system becomes three-stable: a saddle-node bifurcation occurs at $I_{app} = -10$, where a saddle and an unstable node emerge, and at $I_{app} = 40$ a SNLC bifurcation occurs, where the stable node and the saddle collide on the emerging stable limit cycle.

This behaviour can be understood looking at figure (4.9): the nullclines create a narrow channel on the left of the figure and, lowering the current, the fixed points will emerge on the limit cycle. For this reason, at bifurcation, we expect its period will diverge, as confirmed by figure (4.6), the frequency of the limit cycle as a function of the applied current, which is zero at bifurcation point.

In addiction, at $I_{app} = 97.6$, a subcritical Hopf bifurcation occurs and at $I_{app} = 116$ the stable and unstable limit cycles collide and disappear in a saddle-node bifurcation of cycles.

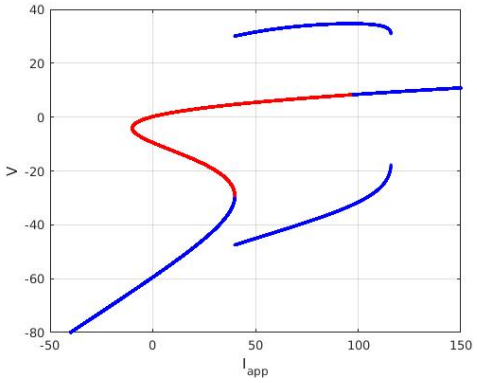

Figura 4.5: Bifurcation diagram in SNLC parameters choice: voltage as a function of applied current. Blue branches are stable and red branches are unstable. The blue branches above and below the fixed points curve correspond to the maximum and minimum voltages along periodic orbits. The blue and red curve in the middle is the fixed points curve.

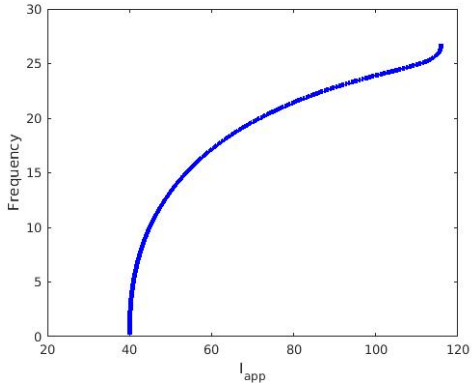

Figura 4.6: Frequency (Hz) as a function of current for stable limit cycles. The zero-frequency limit cycle in $I_{app} = 40$ confirms the SNLC bifurcation and the sudden disappearing of a finite-frequency limit cycle in $I_{app} = 116$ suggests a saddle-node bifurcation of cycles.

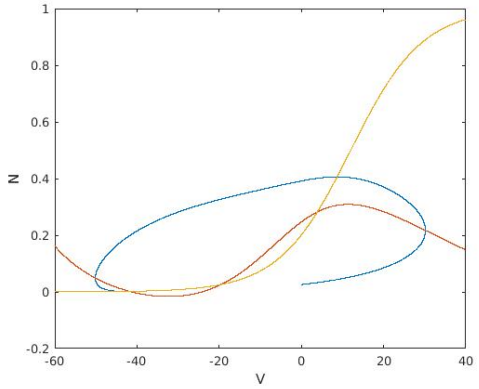

Figura 4.7: Orbit in phase space with nullclines. Here $I_{app} = 30$ and the fixed point is stable. The blue curve is the orbit, the yellow curve is N-nullcline and the red curve is V-nullcline.

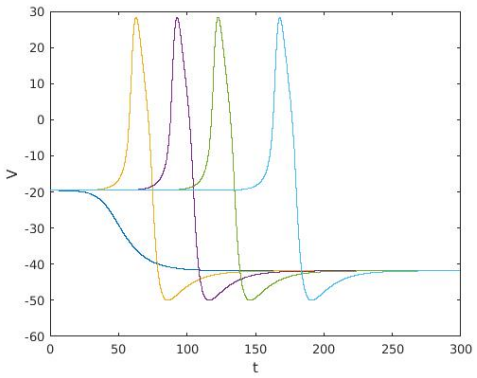

Figura 4.8: V as a function of time. Here $I_{app} = 30$ and the potential approaches a constant value. The delay to spiking can be arbitrary but the spike shape is approximately the same. For the different plots, we start with different initial conditions.

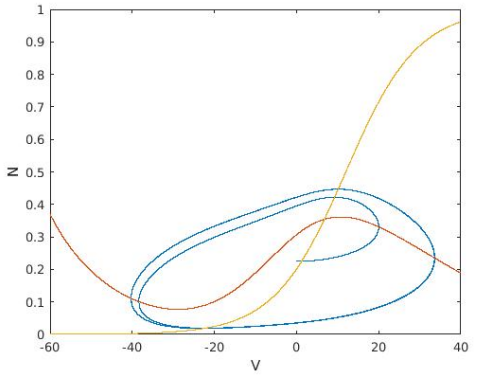

Figura 4.9: Orbit in phase space with nullclines. Here $I_{app} = 70$, the fixed point is unstable and the orbit approaches the stable limit cycle. The blue curve is the orbit, the yellow curve is N-nullcline and the red curve is V-nullcline.

4.3 Saddle-homoclinic bifurcation

This last bifurcation occurs by increasing the parameter Φ and leave all other parameters as in SNLC case, as shown in the Homoclinic column in table (4.1). Since Φ do not affect the nullclines, the number of fixed points is the same as the previous case but their stabilities are different.

The bifurcation diagram in figure (4.10) is similar to the SNLC case, the main difference is that now the saddle collides with the stable limit cycle at bifurcation point $I_{app} \simeq 35$ in a saddle-homoclinic bifurcation. This can be seen by looking at figure (4.14): the orbit is rejected by the unstable node on the right and approaches the stable limit cycle, which is very close to the saddle in the middle.

Note also that the system has three stable attractors in $36.3 < I_{app} < 40.4$: two nodes and a limit cycle. In this range, depending on the initial conditions, the orbits may approach one of them, as shown in figures (4.11), (4.12) and (4.13). I_{app} is a subcritical Hopf bifurcation point, $I_{app} = 40.4$ is a saddle-node bifurcation of cycles point, $I_{app} = -10$ and $I_{app} = 40$ are saddle-node bifurcation points, as in the previous case.

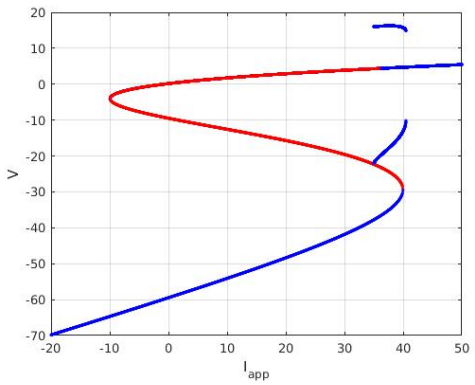

Figura 4.10: Bifurcation diagram in saddle-homoclinic parameters choice: voltage as a function of applied current. Blue branches are stable and red branches are unstable. The blue branches above and below the fixed points curve correspond to the maximum and minimum voltages along periodic orbits. The blue and red curve in the middle is the fixed points curve.

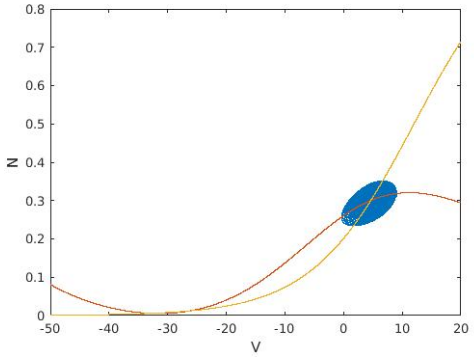

Figura 4.11: Orbit in phase space with nullclines. Here $I_{app} = 39$ and the fixed point on the right is stable, in fact small perturbations are damped and the orbit falls in the fixed point. The blue curve is the orbit, the yellow curve is N-nullcline and the red curve is V-nullcline.

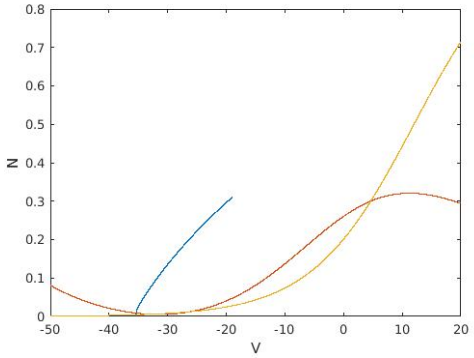

Figura 4.12: Orbit in phase space with nullclines. Here $I_{app} = 39$ and the fixed point on the left is stable but initial conditions are outside the basin of attraction of the stable limit cycle, in fact large the orbit moves away from the limit cycle and falls in the stable fixed point. The blue curve is the orbit, the yellow curve is N-nullcline and the red curve is V-nullcline.

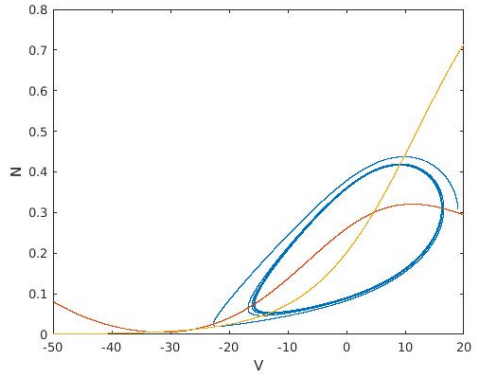

Figura 4.13: Orbit in phase space with nullclines. Here $I_{app} = 39$ and the fixed point is stable but it is surrounded by a small unstable limit cycle and a larger stable limit cycle which attracts the orbit. The blue curve is the orbit, the yellow curve is N-nullcline and the red curve is V-nullcline.

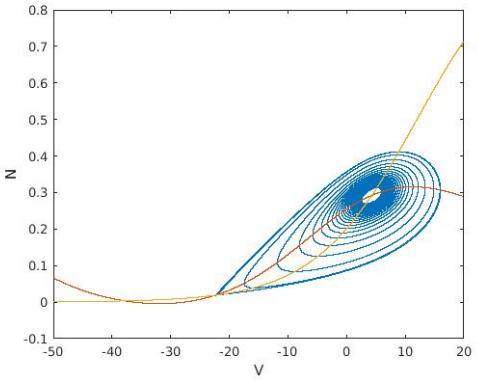

Figura 4.14: Orbit in phase space with nullclines. Here $I_{app} = 35$, which is near to the saddle-homoclinic bifurcation point, where the saddle and the stable limit cycle meet. The blue curve is the orbit, the yellow curve is N-nullcline and the red curve is V-nullcline.

Capitolo 5

Hodgkin-Huxley model

The Hodgkin-Huxley (HH) model has been primarily developed in order to reproduce the behaviour of the membrane potential and of the ionic currents in the squid giant axon. Due to its accuracy, it has yielded a Nobel Prize in Physiology or Medicine in 1963 and it is still exploited as a base for neuronal models.

5.1 The equations of the model

The HH model is defined by four coupled ODEs describing the membrane potential, the sodium and potassium channels and a leakage current. This last current includes all ionic channels that are not explicitly taken into account in the model equations. The model is based on the equivalent electric circuit shown in figure (5.1), which we have already encountered in section 2.3 but we report it once again for convenience, and on the exploitation of the Ohm's law:

$$i_x = \overline{g}_x(V,t)(V - E_x), \tag{5.1}$$

where i_x is the density of current in $\mu A/cm^2$, $\overline{g}_x$ is the density of conductance in mS/cm^2, E_x the resting potential in mV and $x = L,\ K,\ Na$.

After their experiments and analysis, Hodgkin and Huxley proposed the following expressions for the conductances:

$$\begin{aligned} \overline{g}_{Na} &= g_{Na} m^3(V,t) h(V,t), \\ \overline{g}_K &= g_K n^4(V,t), \\ \overline{g}_L &= g_L, \end{aligned} \tag{5.2}$$

where the g_x-s are constants and m, h, n are the gating variables which model the opening of the ionic channels. These three functions are associated to the probability for a gate

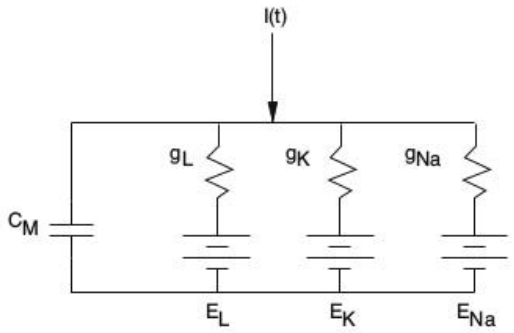

Figura 5.1: Equivalent circuit underlying the Hodgkin-Huxley model [8].

to be open or closed, in fact they satisfy ODEs of this kind:

$$\dot{x} = \alpha_x(V)(1-x) - \beta_x(V)x = \frac{x_\infty(V) - x}{\tau_x(V)}, \tag{5.3}$$

where:

$$\begin{aligned} x_\infty(V) &= \frac{\alpha_x(V)}{\alpha_x(V) + \beta_x(V)}, \\ \tau_x &= \frac{1}{\alpha_x(V) + \beta_x(V)}. \end{aligned} \tag{5.4}$$

$\alpha_x(V)$ and $\beta_x(V)$ are the voltage-dependent rate constants at which a gate goes from the closed to the open and from the open to the closed state, respectively. $\tau_x(V)$ represents the time decay constant and $x_\infty(V)$ is the stationary solution when V is fixed. Finally, the complete model is defined by:

$$\begin{aligned} &C_M\dot{V} = I_{app} - g_{Na}m^3h(V - E_{Na}) - g_Kn^4(V - E_K) - g_L(V - E_L), \\ &\dot{n} = \alpha_n(V)(1-n) - \beta_n(V)n, \\ &\dot{m} = \alpha_m(V)(1-m) - \beta_m(V)m, \\ &\dot{h} = \alpha_h(V)(1-h) - \beta_h(V)h, \end{aligned} \tag{5.5}$$

where:

$$\begin{aligned} &\alpha_n = 0.032(V+52)/(1 - \exp(-(V+52)/5)), \\ &\beta_n = 0.5\exp(-(V+57)/40), \\ &\alpha_m = 0.32(V+54)/(1 - \exp((V+54)/4)), \\ &\beta_m = 0.28(V+27)/(\exp((V+27)/5) - 1), \\ &\alpha_h = 0.128\exp(-(V+50)/18), \\ &\beta_h = 4/(1 + \exp(-(V+27)/5)). \end{aligned} \tag{5.6}$$

C_M is the conductance density of the membrane expressed in $\mu F/cm^2$ and I_{app} is the density of applied current in $\mu A/cm^2$. The parameters values are listed in table (5.1).

Parameter	Value
g_{Na}	120
g_K	36
g_L	0.3
E_{Na}	115
E_K	-12
E_L	10.6
C_M	1

Tabella 5.1: Hodgkn-Huxley parameters. E_{Na}, E_K, E_L are expressed in mV, g_{Na}, g_K, g_L in mS/cm^2, C_M in $\mu F/cm^2$.

5.2 Bifurcation analysis of the model

In figures (5.2) and (5.3) the bifurcation diagram for a HH neuron is shown. A unique fixed point exists for all value of I_{app}, which looses its stability at $I_{app} = 9.78$ in a subcritical Hopf bifurcation and becomes stable again at $I_{app} = 154.5$ in a supercritical Hopf bifurcation. Note that there is a tiny overlap in $6.27 < I_{app} < 9.78$ between the stable fixed point and the stable periodic orbits, as better shown in figure (5.3). In particular, near $I_{app} = 7.88$, there are four limit cycles, which three are unstable and one is stable, which projections in (V, n)-phase plane are shown in figure (5.4).

In the next chapter a mathematical model of the sleep-wake cycle is introduced [1]. The model exploits a Morris-Lecar-like neural network, so this is the reason why we dedicated chapter 4 to the Morris-Lecar model.

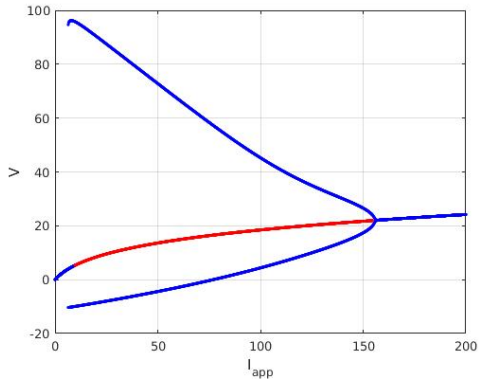

Figura 5.2: Bifurcation diagram: voltage as a function of applied current. Blue branches are stable and red branches are unstable. The blue and red curve in the middle is the fixed-point curve. The blue branches above and below the fixed-point curve correspond to the maximum and minimum voltages along periodic orbits.

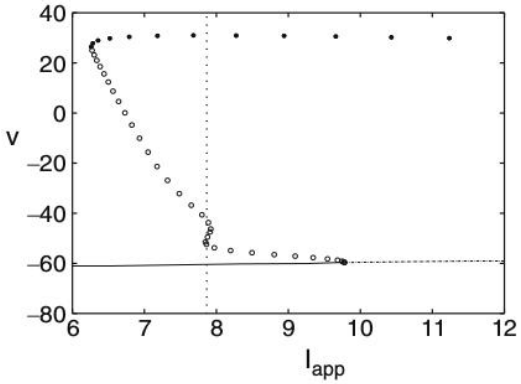

Figura 5.3: Expanded view of (5.2). Full dots are stable orbits, blank dots are unstable orbits [8].

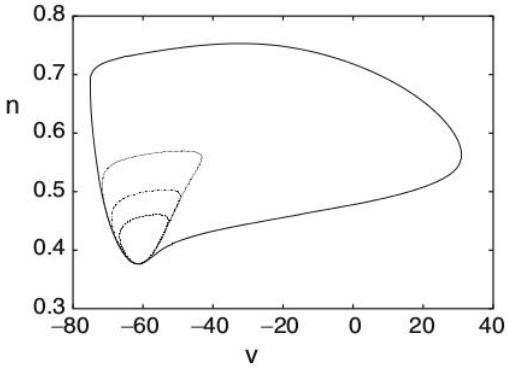

Figura 5.4: (V,n)-phase plane projection of the four limit cycles at $I_{app} = 7.88$ [8].

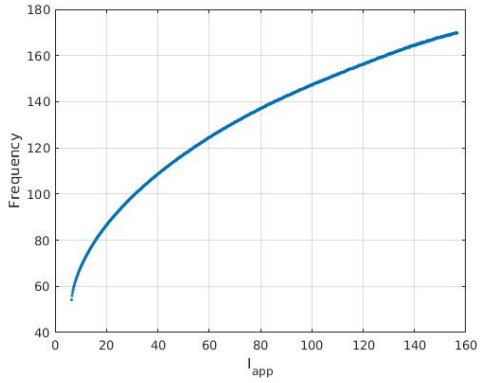

Figura 5.5: Frequency (Hz) as a function of current for stable limit cycles.

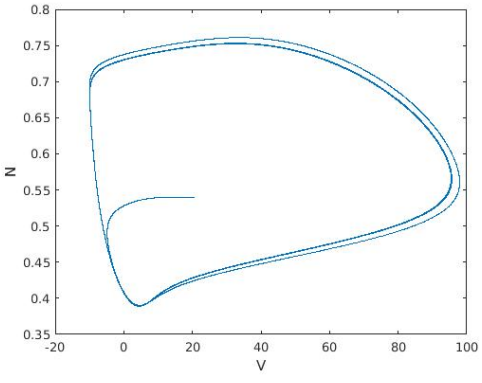

n

Figura 5.6: Orbit in (N,V)-phase plane projection. Here $I_{app} = 10$, the fixed point is unstable and the orbit approaches the stable limit cycle.

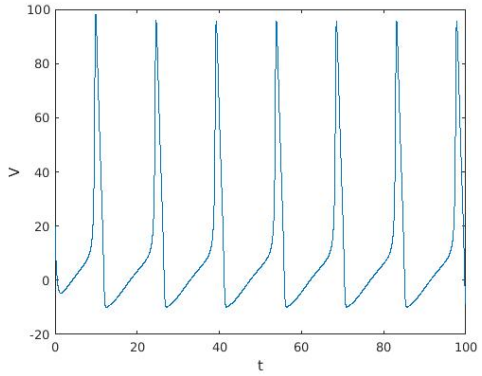

Figura 5.7: V as a function of time. Here $I_{app} = 10$ and the potential is periodic in time.

Capitolo 6

Rempe et al. model

In this chapter we present a biologically-based model of the sleep-wake cycle [1] and its results[1]. This model takes into account some cell groups which play a crucial role in the sleep-wake cycle and is able to reproduce several features of the human sleep-wake cycle. These include timing of sleep and wakefulness (under normal and sleep-deprived conditions), ultradian rhythms, REM and NREM episodes and as well as the narcolepsy due to orexin removal. In this model each cerebral area is described, in a mean field approximation, by a Morris-Lecar-like neuron, with the objectives of providing a mathematical description of the mutual interaction between a circadian pacemaker (C) and a wake-time-dependent homeostatic process (S).

6.1 Description of the model

The model assumes that the regulation of sleep and wake times depends on the interaction between C and S. In particular, process S builds up during wake hours and, when it reaches an upper threshold, the system falls asleep and S decays. On the other hand, when S reaches a lower threshold, the system wakes up and then S increases. These two thresholds varies with time and are regulated by process C. The increase and decrease of S are modelled as exponential functions with different time constants.

The model is based on the sleep-wake switch proposed by Saper et al. [29], in which wake-promoting monoaminergic group (AMIN) and sleep-promoting ventro lateral pre-optic nucleus (VLPO) mutually inhibit, and on the hypothesis that orexinergic cells of the hypothalamus reinforce AMIN to avoid narcolepsy [30]. In addiction, there is also a REM-NREM switch based on the work by Lu et al. [31]: part of the VLPO group, namely its extended portion (eVLPO), inhibits the NREM-promoting cells, while AMIN

[1]Some differences between the equations defined in the paper and the ones that have been defined in the Rempe's code exist and the results are slightly different. In this chapter the equations in Rempe's code are presented and the misprints are outlined.

inhibits the REM-promoting ones. Finally both groups inhibit each other. A scheme of the model circuit is given in figure (6.1).

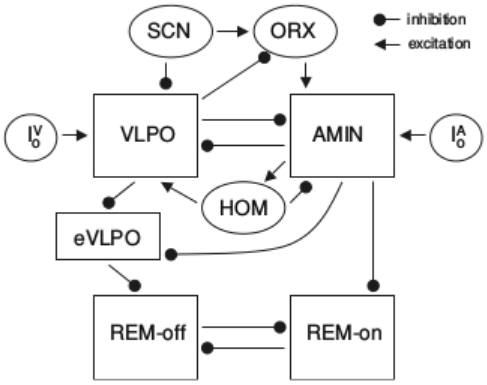

Figura 6.1: A schemata of the model.

6.2 Materials and methods

The presentation of the model is split into two steps. First the sleep-wake flip-flop switch is introduced and then the REM-NREM switch is described. Every term in the equations of the model has explicit functional dependence, otherwise the term is a constant. Parameters values are listed in tables (6.1) and (6.2).

6.2.1 The sleep-wake flip-flop model

The sleep-wake cycle is regulated by the wake-promoting monoaminergic cell groups (AMIN) and by the ventro lateral preoptic region of the hypothalamus (VLPO). These two regions are modelled by:

$$\begin{aligned} \delta_A \dot{x}_A &= f(x_A, y_A) - I_{VLPO}(x_V) + I_{ORX}(x_V, t) + I_0^A - I_{HOM}(t) + I_n^A(t), \\ \dot{y}_A &= g(x_A, y_A), \end{aligned} \tag{6.1}$$

and:

$$\begin{aligned} \delta_V \dot{x}_V &= f(x_V, y_V) - I_{AMIN}(x_A) - I_{SCN}(t) + I_0^V + I_{HOM}(t) + I_n^V(t), \\ \dot{y}_V &= g(x_V, y_V), \end{aligned} \tag{6.2}$$

Parameter	Value
ϵ_A	3
ϵ_V	3
γ_A	5.7
γ_V	3.77
τ_{1A}	1 h
τ_{2A}	2 h
τ_{1V}	1 h
τ_{2V}	2 h
δ_A	0.01
δ_V	0.01
g_{vlpo}	5
g_{amin}	2
g_{scn}	1
I_0^A	3.3
I_0^V	0.45
g_{hom}	5.5
α_h	18.2 1/h
β_h	4.2 1/h
h_{max}	1
g_{noise}	5
a_n	20
w_n	0.01

Tabella 6.1: AMIN-VLPO parameters.

where x_A and x_V are proportional to the the potentials of AMIN and VLPO and represent the respectively overall population activity, and δ_A and δ_V are constants. The variables y_A and y_V are recovery variables. The nonlinear functions f and g are of the form:

$$\begin{aligned} f(x,y) &= 3x - x^3 + 2 - y, \\ g(x,y) &= \epsilon(\gamma H_\infty(x) - y)/\tau(x), \end{aligned} \tag{6.3}$$

where[2] $H_\infty(x) = 1/(1 + exp(-100x))$ is a smooth approximation of the Heaviside step function and $\tau(x) = \tau_1 + (\tau_2 - \tau_1)H_\infty(x)$ has also the shape of a step function. This neuronal model is pretty similar to the Morris-Lecar model, even though is simpler, and will be analysed in the next section.

[2]In the paper $H_\infty(x)$ is defined as $H_\infty(x) = \frac{1}{2}tanh(x)$ instead of (for example) $H_\infty(x) = \frac{1}{2}(tanh(x)+1)$.

The input currents are defined by:

$$\begin{aligned} I_{VLPO} &= g_{vlpo} H_\infty(x_V), \\ I_{AMIN} &= g_{amin} H_\infty(x_A), \\ I_{SCN} &= g_{scn} C(t), \\ I_{ORX} &= I_{SCN}(1 - H_\infty(x_V)), \\ I_{HOM} &= g_{hom} h(t), \end{aligned} \tag{6.4}$$

where $C(t)$ is the circadian pacemaker[3] defined as in [12]:

$$\begin{aligned} C(t) = 2.1 + 0.97 sin(\omega t) + 0.22 sin(2\omega t) + \\ +0.07 sin(3\omega t) + 0.03 sin(4\omega t) + 0.001 sin(5\omega t), \\ \omega = 2\pi/24, \end{aligned} \tag{6.5}$$

which regulates the current coming from SCN, which inhibits the activity of VLPO, and $h(t)$ is defined by the following ODE[4]:

$$\begin{aligned} \dot{h}(t) &= \alpha_h^{-1}(h_{max} - h), \text{ if } x_A > 0, \\ \dot{h}(t) &= -\beta_h^{-1} h, \text{ if } x_A < 0, \end{aligned} \tag{6.6}$$

which means S increases during waking hours and decays during sleep. In the model the orexin current I_{ORX} affects only the activity of AMIN but it is inhibited by VLPO. AMIN and VLPO groups inhibit each other via the currents I_{AMIN} and I_{VLPO}. I_n^A and I_n^V are noisy currents to test the robustness of the model and will be defined in the last section. Finally, I_0^A and I_0^V represent the background cortical drives.

6.2.2 The REM-NREM flip-flop model

The REM-NREM flip-flop switch regulates REM and NREM sleep stages and it is modelled in a similar way indicated in previous section[5]. The equations for the REM-on cells are:

$$\begin{aligned} \delta_R \dot{x}_R &= \sigma\left(f(x_R, y_R) - I_{AMIN}^R(x_A, t) - I_{NREM}(x_N) + I_0^R + I_n^R(t)\right), \\ \dot{y}_R &= \sigma(g(x_R, y_R)), \end{aligned} \tag{6.7}$$

[3] In the paper the constant value 2.1 in the definition of $C(t)$ is missing.

[4] In the paper α_h^{-1} and β_h^{-1} are replaced by α_h and β_h.

[5] In the code $f(x, y)$ in the equations for REM-on and REM-off is defined in a slightly different manner than in the paper. The two definitions coincide if the static currents I_0^R and I_0^N in table (**??**) are redefined as $I_0^R + 1$ and $I_0^N + 1$.

Parameter	Value
ϵ_R	0.3
ϵ_N	0.3
γ_R	6.2
γ_N	6
τ_{1R}	1 h
τ_{2R}	2 h
τ_{1N}	0.5 h
τ_{2N}	1.7 h
δ_R	0.5
δ_N	0.5
σ	11
g_{amin} (AMIN to REM)	2.5
g_{REM}	0.4
g_{NREM}	5
a_e	2
b_e	1
c_e	1.82
c_v	-0.3
g_{evlpo}	6.2
I_0^R	1.1
I_0^N	1.9

Tabella 6.2: REM-NREM parameters.

where[6]:

$$I^R_{AMIN} = g^R_{amin} S(x_A, t), \tag{6.8}$$

$$\dot{S} = \frac{a_S(1-S)}{1+exp(-10x_A)} - b_S S(1 - \frac{1}{1+exp(-10x_A)}), \tag{6.9}$$

while the ones for REM-off cells are:

$$\begin{aligned} &\delta_N \dot{x}_N = \sigma\left(f(x_N, y_N) - I_{eVLPO}(x_e) - I_{REM}(x_R) + I_0^N + I_n^N(t)\right), \\ &\dot{y}_N = \sigma(g(x_N, y_N)), \end{aligned} \tag{6.10}$$

where[7]:

[6]In the paper the equation for $S(t)$ is missing and I^R_{AMIN} is defined as $I^R_{AMIN} = g^R_{amin} H_\infty(x_A)$.

[7]In the paper these two definitions are missing.

$$I_{NREM} = g_{nrem} H_\infty(x_N),$$
$$I_{REM} = g_{rem} H_\infty(x_R),$$

I_0^R and I_0^N are the background drives, I_n^R and I_n^N are noisy currents and the eVLPO activity is described by[8]:

$$\dot{x}_e = -x_e + c_e - a_e h_e(x_V + c_V, k_{xv}) - b_e h_e(x_A, k_{xa})),$$
$$h_e(x,k) = 1/(1 + exp(-x/k)), \tag{6.11}$$

in such away that $I_{eVLPO} = g_{evlpo} x_e$.The functional forms of (6.11) and (**??**) and the corresponding parameters have been chosen in order to reproduce the desired behaviour but are not based on any physiological evidence.

Noise

Noisy currents in each cell group are introduced as:

$$I_n^i = g_{noise} n_i, \tag{6.12}$$
$$\dot{n_i} = w_n(-n_i + a_n N), \tag{6.13}$$

where N is a standard normally distributed random variable, a_n and w_n are constants. At each time step a new value of N is chosen from the normal distribution. Results show the robustness of the model to the noise.

6.3 Results

6.3.1 Normal conditions

A numerical simulation of the system under normal conditions is shown in figure (6.2). The system is awake for approximately 16 hours and asleep for the remaining 8 hours, with rapid transitions (order of 1-2 minutes) between the two states.

In figure (6.3) the activities of REM and NREM nuclei during sleep are shown. The sleep phase begins with a NREM episode and several transitions occur thereafter between REM and NREM phases. In particular, NREM episodes in the early stage of sleep are shorter than the ones in later stages of sleep. These features are in agreement with experimental data [32].

[8] In the paper $h_e(x,k)$ is defined as $h_e(x,k) = \frac{1}{2} tanh(x/k)$ instead of (for example) $h_e(x,k) = \frac{1}{2}(tanh(x/k) + 1)$.

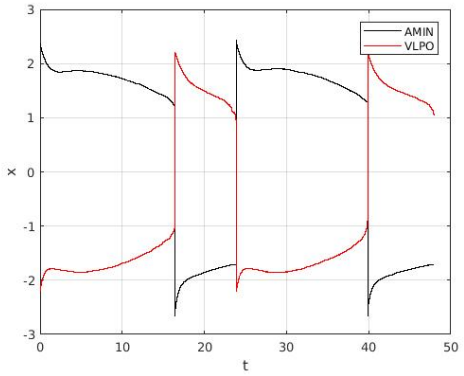

Figura 6.2: Sleeping and waking under normal conditions. Time is measured in hours.

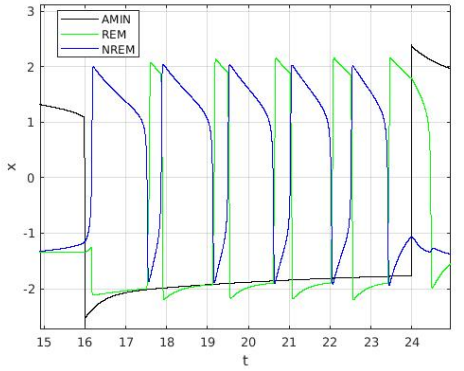

Figura 6.3: REM/NREM cycling during one sleep episode under normal conditions. Time is measured in hours.

6.3.2 Orexin removal

This model is also able to identify the narcolepsy disease by removing the orexin current I_{ORX} from AMIN. We note, looking at figure (6.4), that AMIN shuts down many times while VLPO remains silent. This can be interpreted as wake episodes being interrupted by very short sleep episodes. This is a typical behaviour that occurs in narcolepsy, which is consistent with the hypothesis that orexin stabilizes the sleep-wake cycle.

In addition, looking at figure (6.5), we observe that REM sleep episodes are more frequent than NREMs, due to the loss of orexin [33]. This explains also the occurrence of REM episodes during wake times [34], as shown in figure (6.5).

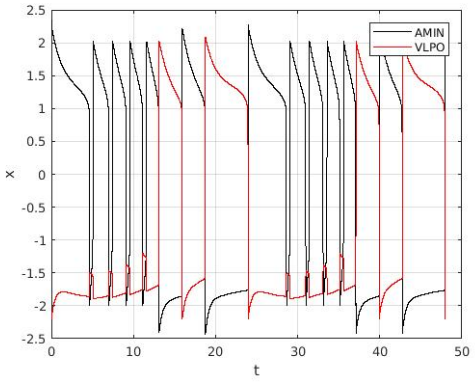

Figura 6.4: Sleeping and waking when orexin is removed. In this case there are several transition into and out of sleep during the day and the night. Time is measured in hours.

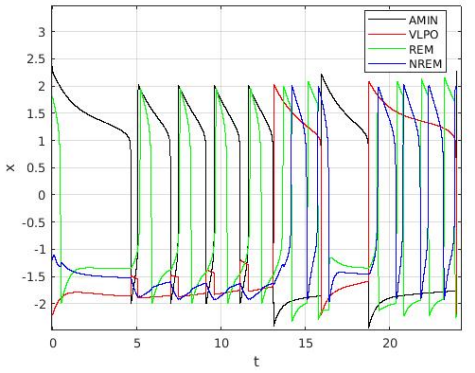

Figura 6.5: REM/NREM cycling when orexin is removed. There are more REM episodes than NREM episodes, including several REM episodes during waking. Time is measured in hours.

6.4 Analysis of single neurons

In this section we analyze the bifurcation diagram of single neurons. Since the functional form is exactly the same for every neuron (equation (6.3)) but parameters depend on the particular kind of population they model (AMIN, VLPO, REM and NREM), the bifurcation diagrams exhibit similarities to each other. In particular, AMIN, REM and NREM, which are shown respectively in figures (6.6), (6.8) and (6.9), present the same identical scheme, so we discuss in detail only AMIN and then VLPO. Here we assume the current I_{app} as the bifurcation parameter, unlike in equation (6.3) where I_{app} is time-dependent. This means that the dynamical system we analyze is:

$$\begin{aligned} \dot{x} &= f(x, y) + I_{app}, \\ \dot{y} &= g(x, y). \end{aligned} \tag{6.14}$$

AMIN bifurcation diagram presents, initially, for $I_{app} < -1.9$, a unique stable fixed point, and then a saddle-node bifurcation occurs so that an unstable node and a saddle emerge. If the applied current is further increased, the system undergoes SNLC bifurcation at $I_{app} = 0$, where a stable node and a saddle collide so that a stable limit cycle emerges surrounding the unstable node. If I_{app} is further increased up to $I_{app} = 1.7$, then another SNLC bifurcation occurs with a stable node and a saddle emerging continuously from the periodic orbit. After this, at $I_{app} = 3.6$, the new saddle and the already-existing unstable node collide in a saddle-node bifurcation, thus leaving only one stable node. are destroyed in a saddle-node bifurcation, then the stable node remains the only fixed point of the system. The only difference between AMIN, REM and NREM bifurcation diagrams is in the values of current at which bifurcations occur.

VLPO bifurcation diagram is even simpler, since only saddle-node bifurcations occur. If $I_{app} < -1.9$, the only fixed point of the system is a stable node, then the first bifurcation occurs and an unstable node and a saddle emerge. Successively, an additional bifurcation occurs at $I_{app} = -0.27$ so that a stable node and a saddle are generated. We note that in the range $-0.27 < I_{app} < 0$ the system has 5 fixed points: 2 saddles, 2 stable nodes and 1 unstable node. At $I_{app} = 0$ a saddle and a stable node collide, and finally, at $I_{app} = 1.63$, unstable node and remaining saddle annihilate, thus leaving a stable node alone.

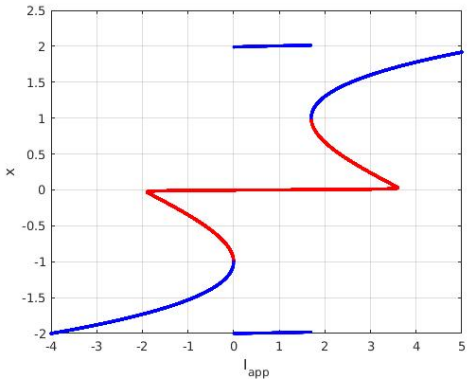

Figura 6.6: Bifurcation diagram for AMIN. AMIN activity as a function of current. Blue branches are stable and red branches are unstable. The blue branches above and below the fixed points curve correspond to the maximum and minimum voltages along periodic orbits. The blue and red curve in the middle is the fixed points curve. $I_1 = -1.9$ is a saddle-node bifurcation point, $I_2 = 0$ and $I_3 = 1.7$ are SNLC bifurcation points, $I_4 = 3.6$ is a saddle-node bifurcation point.

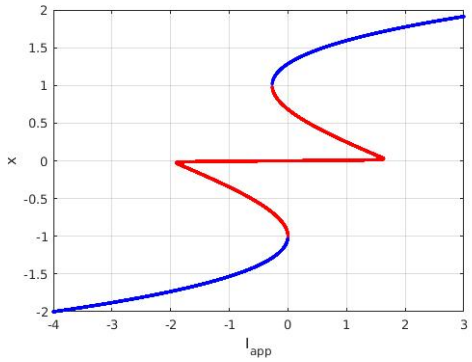

Figura 6.7: Bifurcation diagram for VLPO. VLPO activity as a function of current. Blue branches are stable and red branches are unstable. The blue branches above and below the fixed points curve correspond to the maximum and minimum voltages along periodic orbits. The blue and red curve in the middle is the fixed points curve. $I_1 = -1.9$, $I_2 = -0.27$, $I_3 = 0$ and $I_4 = 1.63$ are all saddle-node bifurcation points.

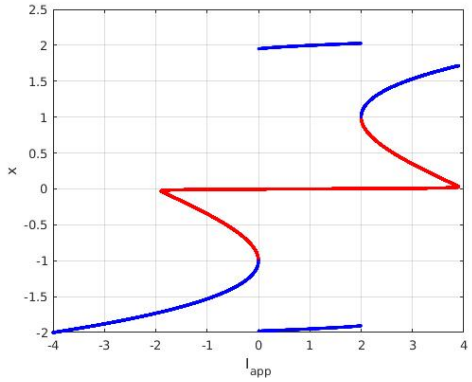

Figura 6.8: Bifurcation diagram for REM. REM activity as a function of current. Blue branches are stable and red branches are unstable. The blue branches above and below the fixed points curve correspond to the maximum and minimum voltages along periodic orbits. The blue and red curve in the middle is the fixed points curve. $I_1 = -1.9$ is a saddle-node bifurcation point, $I_2 = 0$ and $I_3 = 2$ are SNLC bifurcation points, $I_4 = 3.9$ is a saddle-node bifurcation point.

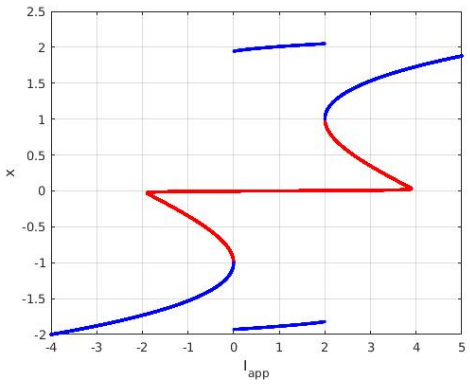

Figura 6.9: Bifurcation diagram for NREM. NREM activity as a function of current. Blue branches are stable and red branches are unstable. The blue branches above and below the fixed points curve correspond to the maximum and minimum voltages along periodic orbits. The blue and red curve in the middle is the fixed points curve. $I_1 = -1.9$ is a saddle-node bifurcation point, $I_2 = 0$ and $I_3 = 2$ are SNLC bifurcation points, $I_4 = 3.9$ is a saddle-node bifurcation point.

Capitolo 7

DSD model

In this chapter we develop a mathematical model of the human sleep-wake cycle, the DSD (D'Agnese, Sarnari and Di Garbo) model, whose grounds are in Rempe et al. model [1]. Our model, still in the mean field approximation, improves on this by taking into account the details of physiology. This improvement is obtained by replacing Morris-Lecar-like neurons with Hodgkin-Huxley ones. In this way a more realistic model is developed, since HH neurons contain a more accurate description of the ionic channels dynamics along with permitting higher accuracy in modelling more realistic synaptic connections.

Despite its basic formulation, the DSD model is able to reproduce the timing of sleep and wakefulness under normal conditions and some features of REM and NREM sleep. Our objective is to demonstrate that it is possible to capture the main features of such a complex system by using a limited number of actors, namely the neurons.

7.1 Description of the model

The model's network is a simplified version than Rempe's one; in fact some cerebral regions are removed, as shown in figure (7.1). In particular, we assume that the main activities of cerebral areas are regulated by the circadian process C by itself, and therefore we remove the homeostatic process S from the network. In addition, in the first simpler model, we did not consider the contribution of orexin to the network. These choices have been made in order to produce an initial simplified version of the model. We outline the model by first introducing the sleep-wake flip-flop switch and then by describing the REM-NREM switch.

7.1.1 The sleep-wake flip-flop model

We follow the observations by Saper et al. [29], and assume that wakefulness is governed by the activity of monoaminergic group AMIN, while sleep phases are principally

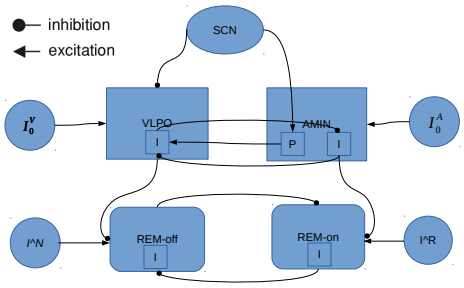

Figura 7.1: A schemata of DSD model.

controlled by the activity of ventro lateral preoptic nucleus VLPO. In agreement with Rempe et al., we assume AMIN to perform both excitatory and inhibitory actions, while VLPO plays only an inhibitory role. As a consequence, AMIN is described by two neurons, a pyramidal and an interneuron, the former excitatory while the latter inhibitory. It follows that AMIN and VLPO interneurons are connected by an inhibitory synapse. The additional excitatory synapse between AMIN pyramidal and VLPO takes into account the removal of the homeostatic process: as shown in figure (6.1), in Rempe et al. model, AMIN excites HOM, which, in turn, excites VLPO. In our model we assume a direct excitatory synapse.

In addition, there is a periodic action of the suprachiasmatic nucleus SCN, which, in spite of the functional form proposed by Achermann and Borbély [12], is described, for the sake of simplicity, as a perfect sinusoidal current. It is not clear yet as SCN has a direct interaction with AMIN interneuron and, for the moment, we assume that SCN is linked only to VLPO interneuron and AMIN pyramidal neuron.

In agreement with the notation adopted in chapter 5, AMIN and VLPO interneurons admit a mathematical description as classical HH neurons [15, 13]:

$$
\begin{aligned}
C\dot{V}_x^I &= I_x^I - g_{Na} {m_x^I}^3 h_x^I (V_x^I - E_{Na}) - g_K {n_x^I}^4 (V_x^I - E_K) - g_L (V_x^I - E_L), \\
\dot{n}_x^I &= \alpha_n(V_x^I)(1 - n_x^I) - \beta_n(V_x^I) n_x^I, \\
\dot{m}_x^I &= \alpha_m(V_x^I)(1 - m_x^I) - \beta_m(V_x^I) m_x^I, \\
\dot{h}_x^I &= \alpha_h(V_x^I)(1 - h_x^I) - \beta_h(V_x^I) h_x^I,
\end{aligned} \tag{7.1}
$$

and:

$$\begin{aligned}
&\alpha_n = 0.032(V+52)/(1-\exp(-(V+52)/5)),\\
&\beta_n = 0.5\exp(-(V+57)/40),\\
&\alpha_m = 0.32(V+54)/(1-\exp((V+54)/4)),\\
&\beta_m = 0.28(V+27)/(\exp((V+27)/5)-1),\\
&\alpha_h = 0.128\exp(-(V+50)/18),\\
&\beta_h = 4/(1+\exp(-(V+27)/5)),
\end{aligned} \tag{7.2}$$

where I_x^I is the applied current to interneuron x = AMIN, VLPO.

AMIN pyramidal neuron is modelled as an HH with an additional ionic channel [15, 13]:

$$\begin{aligned}
&C\dot{V_x^P} = I_x^P - g_{Na}m_x^3h_x(V_x^P - E_{Na}) - g_K n_x^4(V_x^P - E_K) - g_L(V_x^P - E_L) - g_M w_x(V_x - V_M),\\
&\dot{n_x^P} = \alpha_n(V_x^P)(1-n_x^P) - \beta_n(V_x^P)n_x^P,\\
&\dot{m_x^P} = \alpha_m(V_x^P)(1-m_x^P) - \beta_m(V_x^P)m_x^P,\\
&\dot{h_x^P} = \alpha_h(V_x^P)(1-h_x^P) - \beta_h(V_x^P)h_x^P,\\
&\dot{w_x} = \frac{w_{\infty,x} - w_x}{\tau_w},
\end{aligned} \tag{7.3}$$

and:

$$\begin{aligned}
&\alpha_n = 0.032(V+52)/(1-\exp(-(V+52)/5)),\\
&\beta_n = 0.5\exp(-(V+57)/40),\\
&\alpha_m = 0.32(V+54)/(1-\exp((V+54)/4)),\\
&\beta_m = 0.28(V+27)/(\exp((V+27)/5)-1),\\
&\alpha_h = 0.128\exp(-(V+50)/18),\\
&\beta_h = 4/(1+\exp(-(V+27)/5)),\\
&\tau_w = 400/(3.3\exp((V+35)/20)+\exp(-(V+35)/20)),\\
&w_{\infty,x} = 1/(1+\exp(-(V+35)/10)),
\end{aligned} \tag{7.4}$$

where I_x^P is the applied current to pyramidal neuron x = AMIN.

Finally, the applied currents are defined by:

$$\begin{aligned}
&I_{AMIN}^I = J_{VLPO}^I + I_{AMIN}^0,\\
&I_{VLPO}^I = I_{SCN}(t) + J_{AMIN}^P + J_{AMIN}^I + I_{VLPO}^0,\\
&I_{AMIN}^P = I_{SCN}(t) + I_{AMIN}^0,
\end{aligned} \tag{7.5}$$

where:

$$
\begin{aligned}
&I_{SCN} = I^0_{SCN} \sin(2\pi/T),\\
&J^I_{AMIN} = -g_I S_{AMIN}(V_{VLPO} - V_{FF}),\\
&J^I_{VLPO} = -g_I S_{VLPO}(V_{AMIN} - V_{FF}),\\
&J^P_{AMIN} = -g_{PF} S_{AMIN}(V_{VLPO} - V_{PF}).
\end{aligned} \tag{7.6}
$$

T is the period and I^0_x are constants, x = AMIN, VLPO, SCN. The dynamics of the chemical synapses is given by:

$$
\begin{aligned}
&\dot{S}_{VLPO} = 2\left(1 + \tanh(\frac{V_{VLPO}}{4})\right)(1 - S_{VLPO}) - \frac{S_{VLPO}}{\tau_2},\\
&\dot{S}^P_{AMIN} = 5\left(1 + \tanh(\frac{V^P_{AMIN}}{4})\right)(1 - S^P_{AMIN}) - \frac{S^P_{AMIN}}{\tau_1},\\
&\dot{S}^I_{AMIN} = 2\left(1 + \tanh(\frac{V^I_{AMIN}}{4})\right)(1 - S^I_{AMIN}) - \frac{S^I_{AMIN}}{\tau_2}.
\end{aligned} \tag{7.7}
$$

All parameter values are listed in table (7.1). We observe that replacing the Morris-Lecar-like neuron equations with the HH ones causes, even at single neuron level, a big increase in the complexity of the problem. In fact, the HH system can exhibit a huge variety of dynamical behaviours, including spatio-temporal chaos, due to violation of the Poincaré-Bendixson theorem.

7.1.2 The REM-NREM flip-flop switch

REM and NREM groups exhibit mutual inhibition and are also inhibited by AMIN and VLPO interneurons, respectively. As a consequence, also REM and NREM are both described as interneurons. As mentioned before, the dynamics of REM and NREM is influenced by AMIN and VLPO but it is not true the other way around, namely that REM and NREM produce alterations in the dynamics of AMIN and VLPO. It follows that the first logical step to study REM-NREM switch consists in determining the optimal parameters for AMIN-VLPO switch. As shown in figure (7.1), the extended nuclei of VLPO (eVLPO) are removed from the model and VLPO itself directly affects the dynamics of NREM group. Therefore, the model equations are:

$$
\begin{aligned}
&C\dot{V^I_x} = I^I_x - g_{Na} {m^I_x}^3 h^I_x (V^I_x - E_{Na}) - g_K {n^I_x}^4 (V^I_x - E_K) - g_L(V^I_x - E_L),\\
&\dot{n^I_x} = \alpha_n(V^I_x)(1 - n^I_x) - \beta_n(V^I_x) n^I_x,\\
&\dot{m^I_x} = \alpha_m(V^I_x)(1 - m^I_x) - \beta_m(V^I_x) m^I_x,\\
&\dot{h^I_x} = \alpha_h(V^I_x)(1 - h^I_x) - \beta_h(V^I_x) h^I_x,
\end{aligned} \tag{7.8}
$$

Parameter	Value
g_{Na}	100
g_K	80
g_L	0.15
E_{Na}	50
E_K	-100
E_L	-72
C	1
g_I	0.25
g_{PF}	0.3
g_M	1
V_M	-100
V_{FF}	0
V_{PF}	-80
τ_1	2
τ_2	10

Tabella 7.1: DSD parameters. $E_{Na}, E_K, E_L, V_M, V_{FF}, V_{PF}$ are expressed in mV, g_x-s in mS/cm^2, C in $\mu F/cm^2$, τ_1, τ_2 in ms.

and:

$$\begin{aligned}
&\alpha_n = 0.032(V+52)/(1-\exp(-(V+52)/5)),\\
&\beta_n = 0.5\exp(-(V+57)/40),\\
&\alpha_m = 0.32(V+54)/(1-\exp((V+54)/4)),\\
&\beta_m = 0.28(V+27)/(\exp((V+27)/5)-1),\\
&\alpha_h = 0.128\exp(-(V+50)/18),\\
&\beta_h = 4/(1+\exp(-(V+27)/5)),
\end{aligned} \tag{7.9}$$

where $x =$ REM, NREM and the applied currents are defined by:

$$\begin{aligned}
&I^I_{REM} = I^0_{REM} + J^I_{NREM} + J^I_{AMIN},\\
&I^I_{NREM} = I^0_{NREM} + J^I_{REM} + J^I_{VLPO},
\end{aligned} \tag{7.10}$$

and:

$$
\begin{aligned}
J^I_{AMIN} &= -\frac{1}{2} g_I S^I_{AMIN}(V^I_{REM} - V_{FF}),\\
J^I_{NREM} &= -\frac{1}{2} g_I S^I_{NREM}(V^I_{REM} - V_{FF}),\\
J^I_{REM} &= -\frac{1}{2} g_I S^I_{REM}(V^I_{NREM} - V_{FF}),\\
J^I_{VLPO} &= -\frac{1}{2} g_I S^I_{VLPO}(V^I_{NREM} - V_{FF}),
\end{aligned} \tag{7.11}
$$

while the dynamics of REM-NREM synapses are given by:

$$
\begin{aligned}
\dot{S}^I_{NREM} &= 2\left(1 + \tanh(\frac{V^I_{NREM}}{4})\right)(1 - S^I_{NREM}) - \frac{S^I_{NREM}}{\tau_2},\\
\dot{S}^I_{REM} &= 2\left(1 + \tanh(\frac{V^I_{REM}}{4})\right)(1 - S^I_{REM}) - \frac{S^I_{REM}}{\tau_2}.
\end{aligned} \tag{7.12}
$$

7.2 Results

In this section we show the results of numerical simulations. In particular, we note that it would be impossible to understand completely the dynamics of the system by simply looking at a V vs. t plot, for large values of t, namely of the order of one or more days. This is due to the fact that the action potentials of HH occur on a much faster time scale, typically of the order of a few milliseconds. We overcome this problem by analyzing raster plots of the system. A raster plot is a typical way to detect action potentials spikes, where each spike is represented by a dot in a plane, as time varies. This is an easy way to see whether a neuron is firing or not.

An additional problem is given by the fact that, in order to have a good resolution, the time step must be chosen very small. This means that, since the simulation must last, in principle, at least 24 hours, a huge computational time is required. This can be avoided noting that the system has two time scales, the neuronal oscillations and the period of the circadian pacemaker. Since the orbits in a HH approach a stable fixed point or limit cycle in a time much smaller than the one in which the current due to SCN varies appreciably, we assume that, if the period of the circadian pacemaker T is much longer than the transient time t_T in which the orbit stabilizes, we can define a new period and interpret it as a rescaling of the original 24-hours period.

An estimate for t_T is obtained by removing the circadian pacemaker from the system and look at the time required for the system stabilize. Looking at figure (7.2), we see that spikes become regular after a transient time $t_T \approx 200ms$, thus, to ensure $t_T \ll T$, we assume $T = 3000ms$. Finally, the parameters of the model are chosen in such a way that VLPO is active 1/3 of the period while AMIN is silent. By contrast, AMIN is active

2/3 of the period, while VLPO is silent. A sample raster plot of sleep-wake cycle under normal conditions is shown in figure (7.3).

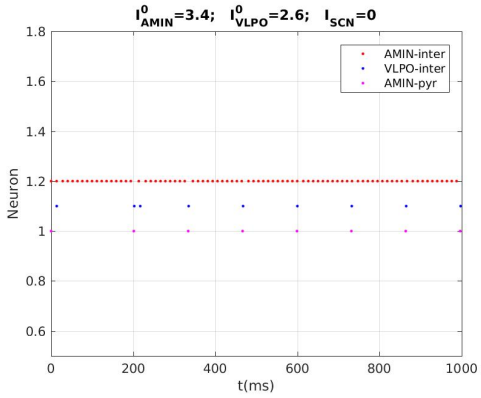

Figura 7.2: Here the system has no circadian pacemaker input due to the suprachiasmatic nucleus ($I_{SCN} = 0$) and the pattern of the spikes becomes regular after a transient of the order of 200 ms. Note that when AMIN-P spikes also VLPO does and VLPO inhibits AMIN-I for a fraction of second.

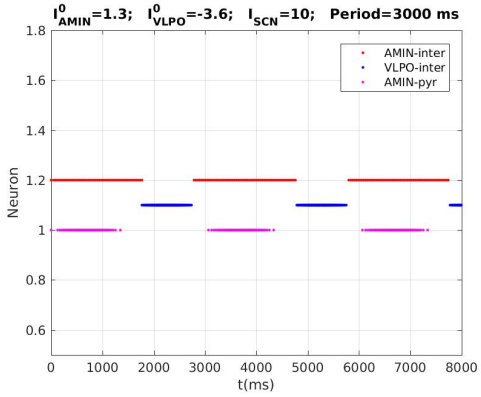

Figura 7.3: In this sample the amplitude of the sinusoidal current system due to the suprachiasmatic nucleus is $I_{SCN} = 10\ nA$. VLPO is active 1/3 of the period and AMIN is active 2/3 of the period with no overlapping.

7.2.1 $(I^0_{SCN}, I^0_{AMIN}, I^0_{VLPO})$ parameters-space

The desired behaviour of the system can be obtained by different combinations of parameters I^0_{SCN}, I^0_{AMIN} and I^0_{VLPO}. This set define a solid in $\mathbf{R}^3$, which is represented in figures (7.4) by keeping fixed a value for I_{SCN} and projecting on (I^0_{AMIN}, I^0_{VLPO})-plane. If a point contained in that solid is chosen, then the system behaves as in figure (7.3).

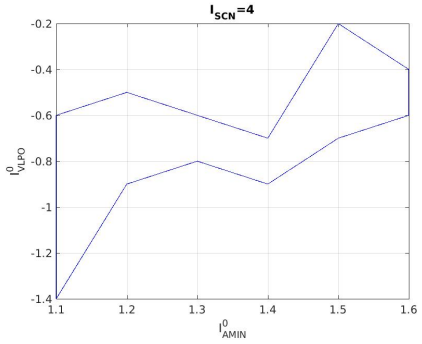

((a)) $I^0_{SCN} = 4$

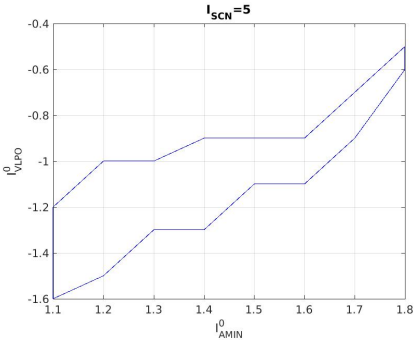

((b)) $I^0_{SCN} = 5$

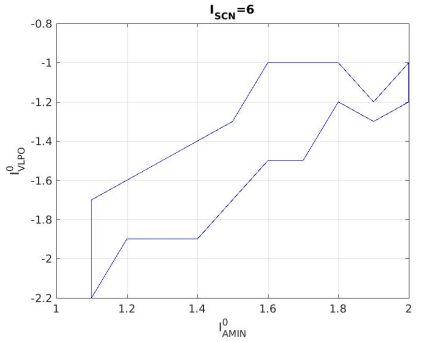

((a)) $I^0_{SCN} = 6$

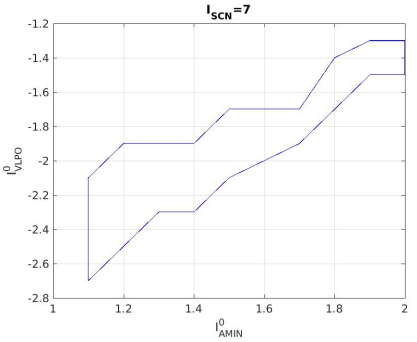

((b)) $I^0_{SCN} = 7$

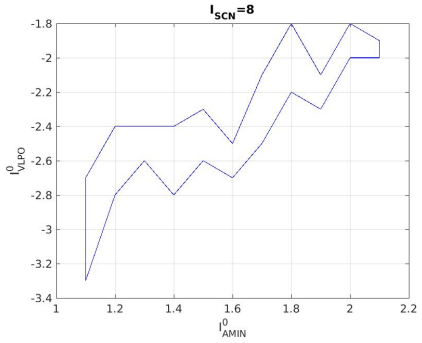

((a)) $I^0_{SCN} = 8$

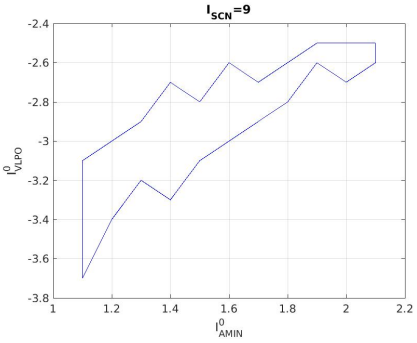

((b)) $I^0_{SCN} = 9$

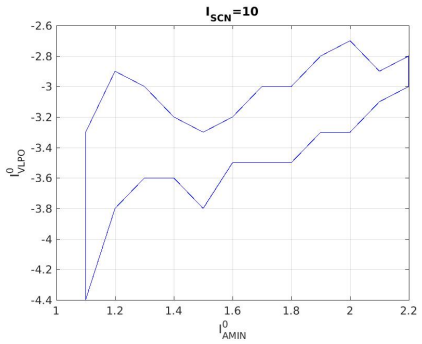

((a)) $I^0_{SCN} = 10$

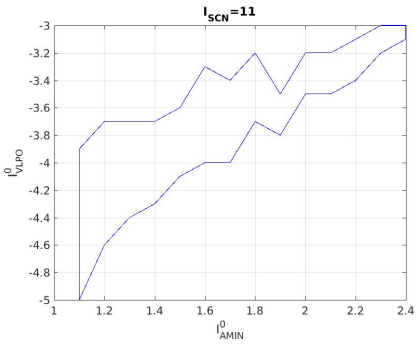

((b)) $I^0_{SCN} = 11$

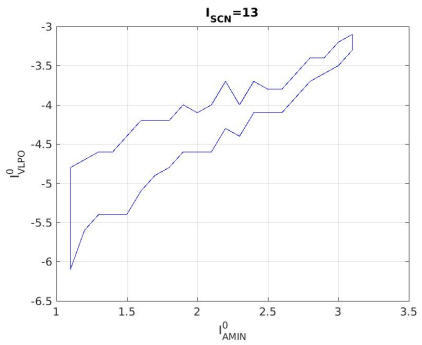

((a)) $I^0_{SCN} = 13$

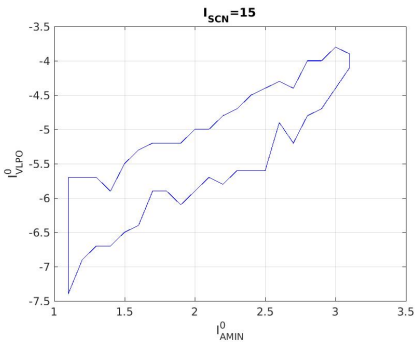

((b)) $I^0_{SCN} = 15$

Figura 7.4: The internal area in parameters-space represents the combinations such that AMIN is active 2/3 of the period and VLPO is active 1/3 of the period.

7.2.2 I^0_{REM} and I^0_{NREM} parameters choice

In order to complete the study of the model under normal conditions, we have to find a suitable combination for I^0_{REM} and I^0_{NREM}. Since REM-NREM-nuclei are influenced by but do not influence AMIN/VLPO-nuclei (i.e. there is no feedback), I^0_{REM} and I^0_{NREM} can be chosen after we have fixed I^0_{AMIN} and I^0_{VLPO}.

Since the dynamics underlying the interactions between SCN, AMIN and VLPO is poorly understood, there are no particular reasons for choosing a special combination for the values of I^0_{SCN}, I^0_{AMIN} and I^0_{VLPO}.

Choosing, for example, the triplet ($I^0_{SCN} = 10$, $I^0_{AMIN} = 1.4$ and $I^0_{VLPO} = -3.4$), the system behaves as shown in figure (7.5). The most relevant feature is that REM group is active during all sleeping phase, while NREM group is silent. On the other hand, NREM group is active during wakefulness, while REM is silent. This behaviour is not in agreement with experiments: REM and NREM groups should be always silent during wakefulness and active during sleep. Since this behaviour is spread all over the allowed values of I^0_{SCN}, I^0_{AMIN} and I^0_{VLPO}, namely the ones defined by figure (7.4), then the model, as it is currently, is not able to reproduce accurately the whole REM-NREM dynamics. In order to avoid this, it has been tried to modify the conductances' values in the VLPO-NREM and AMIN-REM synaptic connections, but the qualitative behaviour did not change.

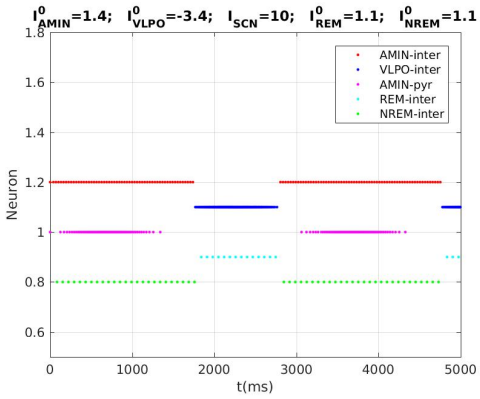

Figura 7.5: A sample raster plot of the complete DSD model.

Capitolo 8

Conclusions and further developments

In this work we developed a biologically-based mathematical model able to reproduce some features of the human sleep-wake cycle. These features include the timing of sleep and wakefulness under normal conditions and part of the occurrence of REM episodes during the sleep.

We began from the observation by Saper et al. [29], who proposed a sleep-wake flip-flop switch, in which wake-promoting monoaminergic group AMIN is linked to sleep-promoting ventro lateral preoptic group VLPO via inhibitory connection, and from the further work by Lu et al. [31], in which the initial model is extended to include REM and NREM dynamics.

These particular features are collected by Phillips and Robinson in their model [19], which is as able to reproduce some behaviours occurring in the sleep-wake cycle, such as the timing of sleep and wakefulness and the activities of REM and NREM nuclei, but the description is weak from a physiological point of view. This is due to the fact that the equations that model the dynamics are phenomenological.

Subsequently, Rempe et al. develop a more realistic mathematical model [1] which is able to reproduce several features of the human sleep-wake cycle, by describing cerebral areas as Morris-Lecar-like neurons, in a mean field approximation. The model takes into account many ingredients that play an important role in the sleep-wake cycle, such as the stabilizing effect of orexin on the sleep-wake mechanism and the interaction between the circadian pacemaker and the homeostatic process, following the hypothesis by Achermann and Borbély [4]. However, there are still some assumptions which do not have solid grounds in physiology, for example the parameters choice is made in order to reach the desired behaviours but it is not based on physiological variables. In addiction, the type of neuronal model chosen and the synaptic connections are not realistic, because they do not describe accurately the underlying dynamics.

In our work, the neural network circuit is much simpler than the one adopted by Rempe, in fact some cerebral areas and the homeostatic process are removed but, on the other hand, the neuronal model is very accurate and realistic, namely the Hodgkin-Huxley model [3], and also the synaptic connections are biologically-based [15, 13]. Despite its simplicity, the model is able to reproduce the main features of sleep-wake cycle under normal conditions, such as the timing of sleep and wakefulness and part of the REM-NREM activity.

This particular approach is hopefully promising. It demonstrates that is possible to describe some features of a huge and complex network only using a few number of neurons. This means that a mean field approximation of cerebral areas is obtainable even by using a single neuron, thus this can reduce the complexity of the network. In addition, there is a much more detailed description of ionic channels and synaptic connections, thus it would be possible to describe perturbations of any kind, such as the effect of drugs, which may affect ionic channels or synapses, and of diseases which are related to dysfunctions of sleep-wake cycle, such as epilepsy [23, 25].

This particular model we developed is extremely simple and, since there is a lack in reproducing REM and NREM dynamics, a deeper investigation is required. Subsequently, the next improvement could be extend the model in order to include the processes that are not taken into account, mainly the homeostatic process and the orexin dynamics. After this, the mean field approximation can be further improved by describing the already-present cerebral using more neurons and additional synaptic connections. However, these further developments requires a much more detailed knowledge, which is still missing, of the structure of the brain network, namely the kind of cells which compose the cerebral areas and the precise connections among them. We hope, therefore, that our work would open a new series of experiments addressed to deepen our interest about the underlying dynamics of the sleep-wake cycle, which is still poorly understood.

Appendice A

Numerical methods

Numerical methods are an essential tool for the study of nonlinear dynamical systems, because analytical solutions are extremely rare. In this section the main techniques which has been used for our work are presented.

A.1 Newton's method

Newton's Method in n dimensions allows us to find the roots of an n-dimensional nonlinear system of equations. If we are looking for the fixed points of a system of nonlinear ODEs, this method works as well. Anyway in some particular cases it is possible to use Newton's Method in $n - m$ dimensions, which is much less expensive computationally than the n-dimensional version, and a brief proof is soon provided.

A.1.1 Newton's method in one dimension

Let us suppose we have to find a root x^* of the equation:

$$f(x^*) = 0. \tag{A.1}$$

It can be shown the recurrence equation:

$$x_{n+1} = x_n - \frac{f(x_n)}{f'(x_n)}, \tag{A.2}$$

converges to x^* if a suitable initial condition x_0 is set and $f'(x^*) \neq 0$. This algorithm can be generalized for n dimensions.

A.1.2 Dimensions reduction

Let us suppose we are looking for the fixed points of a 2-dimensional nonlinear system of the form:

$$\begin{aligned} \dot{x} &= f(x, y), \\ \dot{y} &= g(x, y), \end{aligned} \tag{A.3}$$

and setting $\dot{x} = \dot{y} = 0$ let us suppose g can be simplified as:

$$g(x^*, y^*) = 0 \Longrightarrow y^* = \bar{g}(x^*), \tag{A.4}$$

hence substituting in f we get:

$$f(x^*, y^*) = f(x^*, \bar{g}(x^*)) \equiv F(x^*) = 0. \tag{A.5}$$

This means (A.5) can be solved using Newton's Method in one dimension and substituting in (A.4) allows to find the fixed points (x^*, y^*). In general a n-dimensional system, when is possible to express m variables as a function of the other variables, can be solved by using a $(n - m)$-dimensional finding-roots algorithm.

A.2 Numerical solution of ODEs

Since the ODEs we are dealing with are nonlinear, often an analytic solution is not available so a numerical solution is necessary. The general idea is to perform a discretization of ODEs and solve the associated recurrence equations. In this section two of the most common algorithms to solve ODEs numerically are presented.

A.2.1 Euler's method

Euler's method is the simplest algorithm to solve ODEs. It is based on 1st order Taylor's expansion.

Given a dynamical system of the form:

$$\dot{\vec{x}} = \vec{\Phi}(\vec{x}, t), \tag{A.6}$$

and expanding it in Taylor's series we get:

$$\vec{x}(t + \Delta t) = \vec{x}(t) + \Delta t \vec{\Phi}(\vec{x}, t) + \vec{e}_n. \tag{A.7}$$

The method consists in neglecting the remainder $\vec{e}$:

$$\vec{x}_{n+1} = \vec{x}_n + \Delta t \vec{\Phi}(\vec{x_n}, t_n). \tag{A.8}$$

In this case is pretty obvious that the local error committed by the algorithm at time step t_n is given by:

$$||\vec{e}_n|| = ||\vec{x}(t_n) - \vec{x}_n|| = O(\Delta t^2). \tag{A.9}$$

A.2.2 Runge-Kutta 4th order method

Runge-Kutta 4th order method is one the most used algorithm, because of its accuracy and relative simplicity.

Given a non-autonomous dynamical system of the form:

$$\dot{\vec{x}} = \vec{\Phi}(\vec{x}, t), \tag{A.10}$$

Runge-Kutta 4th order method consists in the recurrence equation:

$$\vec{x}_{n+1} = \vec{x}_n + \frac{\Delta t}{6}\left(\vec{K_1} + 2\vec{K_2} + 2\vec{K_3} + \vec{K_4}\right), \tag{A.11}$$

where:

$$\begin{aligned}
\vec{K_1} &= \vec{\Phi}(\vec{x_n}, t_n), \\
\vec{K_2} &= \vec{\Phi}(\vec{x_n} + \frac{\Delta t}{2}\vec{K_1}, t_n + \frac{\Delta t}{2}), \\
\vec{K_3} &= \vec{\Phi}(\vec{x_n} + \frac{\Delta t}{2}\vec{K_2}, t_n + \frac{\Delta t}{2}), \\
\vec{K_4} &= \vec{\Phi}(\vec{x_n} + \Delta t\vec{K_3}, t_n + \Delta t).
\end{aligned} \tag{A.12}$$

In general the local error committed by a mth order algorithm in a single step at time t_n is expressed by:

$$e_n = ||\vec{x}(t_n) - \vec{x}_n|| = O(\Delta t^{m+1}), \tag{A.13}$$

and in this case it can be shown we have $e_n = O(\Delta t^5)$.

Bibliografia

[1] Rempe, M. J., Best, J., Terman, D.: *A mathematical model of the sleep/wake cycle.* J. Math. Biol. 2010 60: 615-644.

[2] Strogatz S. H.: *Human sleep and circadian rhythms: a simple model based on two coupled oscillators.* J. Math. Biol. 1987 Winter; 2(4): 317-29.

[3] Hodgkin A. L., Huxley A. F.: *A quantitative description of membrane current and its application to conduction and excitation in nerve.* J. Physiol. 1952 Aug 28; 117(4): 500–544.

[4] Borbély A. A.: *A two process model of sleep regulation.* Hum. Neurobiol. 1982; 1(3): 195-204.

[5] Borbély A. A., Daan S., Wirz-Justice A., Deboer T.: *The two-process model of sleep regulation: a reappraisal.* J. Sleep Res. 2016 Apr; 25(2): 131-43.

[6] Saiki Y.: *Numerical detection of unstable periodic orbits in continuous-time dynamical systems with chaotic behaviors.* Nonlin. Processes Geophys., 14, 615–620, 2007.

[7] Strogatz S. H.: *Nonlinear Dynamics and Chaos: With Applications to Physics, Biology, Chemistry, And Engineering.* CRC Press, 2000.

[8] Ermentrout G. B, Terman D. H.: *Mathematical Foundations of Neuroscience.* Springer, 2010.

[9] Parker T. S., Chua L. O.: *Practical Numerical Algorithms for Chaotic Systems.* Springer-Verlag, 1989.

[10] Morris C., Lecar H.: *Voltage oscillations in the barnacle giant muscle fiber.* Biophys. J. 1981 Jul;35(1):193-213.

[11] Héricé C., Patel A. A., Sakata S.: *Circuit mechanisms and computational models of REM sleep.* Neurosci. Res. 2019 Mar;140:77-92.

[12] Achermann P., Borbély A. A.: *Simulation of daytime vigilance by the additive interaction of a homeostatic and a circadian process.* Biol. Cybern 1994; 71(2): 115-121.

[13] Olufsen M.S., Whittington M.A., Camperi M., Kopell N.: *Simulation of daytime vigilance by the additive interaction of a homeostatic and a circadian process.* J Comput Neurosci. 2003 Jan-Feb;14(1):33-54.

[14] S. Chillemi, M. Barbi, A. Di Garbo: *A network of pyramidal neurons is sensitive to the timing of its excitatory inputs.* Neurocomputing 74 (2011) 1159–1164.

[15] F. Vallone ,A. Cintio, S. Chillemi, A. Di Garbo: *Thalamic inputs modulate cortical activity: Possibility to control the generation and the termination of seizure-like behaviour.* Neurocomputing 151 (2015) 34–48.

[16] R. D. Gleit, C. G. Diniz Behn, V. Booth: *Modeling Interindividual Differences in Spontaneous Internal Desynchrony Patterns.* Journal of Biological Rhythms, Vol. 28 No. 5, (2013) 339-355.

[17] G. Turchetti: *Modelli e Metodi Numerici della Fisica.* Department of Physics and Astronomy, University of Bologna, 2017.

[18] McCarley R.W., Hobson J.A.: *Neuronal excitability modulation over the sleep cycle: a structural and mathematical model.* Science. 189(4196):58-60. 1975.

[19] Phillips A.J.K., Robinson P.A.: *A Quantitative Model of Sleep-Wake Dynamics Based on the Physiology of the Brainstem Ascending Arousal System.* Journal of Biological Rhythms, 22(2), 167–179. 2007.

[20] L. R. Squire, D. Berg, F. E. Bloom, S. du Lac, A. Ghosh, N. C. Spitzer: *Fundamental Neuroscience.* Academic Press, 2012.

[21] R. E. Brown, R. Basheer, J.T. McKenna, R. E. Strecker, R. W. McCarley: *Control of Sleep and Wakefulness.* Physiol Rev. 2012 Jul; 92(3): 1087-187.

[22] T. E. Scammell, E. Arrigoni, J. O. Lipton: *Neural Circuitry of Wakefulness and Sleep.* Neuron, Volume 93, Issue 4, 22 February 2017, Pages 747-765

[23] Van Erum J., Van Dam D., De Deyn P.P.: *Sleep and Alzheimer's disease: A pivotal role for the suprachiasmatic nucleus.* Sleep Med Rev. 2017 Jul 28.

[24] Scammell T. E.: *Overview of sleep: the neurologic processes of the sleep-wake cycle.* J Clin Psychiatry. 2015 May;76(5):e13.

[25] Lim M.M., Gerstner J.R., Holtzman D.M.: *The sleep-wake cycle and Alzheimer's disease: what do we know?* Neurodegener Dis Manag. 2014;4(5):351-62.

[26] Ono D., Yamanaka A.: *Hypothalamic regulation of the sleep/wake cycle.* Neurosci Res. 2017 May;118:74-81.

[27] C. Stangor: *Introduction to Psychology.* Flat World Knowledge, L.L.C. (2011).

[28] Y. Kuznetzov: *Elements of Applied Bifurcation Theory.* Springer-Verlag New York, (2004).

[29] Saper C. B., Chou T. C., Scammell T. E.: *The sleep switch: hypothalamic control of sleep and wakefulness.* Trends Neurosci. 2001 Dec;24(12):726-31.

[30] Saper C. B., Scammell T. E., Lu J.: *Hypothalamic regulation of sleep and circadian rhythms.* Nature. 2005 Oct 27;437(7063):1257-63.

[31] Lu J., Sherman D., Devor M., Saper C. B.: *A putative flip–flop switch for control of rem sleep.* Nature. 2006; 441(7093):589–594

[32] Swick T.J.: *The neurology of sleep.* Neurol Clin. 2005; 23(4):967–989

[33] Boeve BF, Silber MH, Saper CB, Ferman TJ, Dickson DW, Parisi JE, Benarroch EE, Ahlskog JE, Smith GE, Caselli RC, Tippman-Peikert M, Olson EJ, Lin SC, Young T, Wszolek Z, Schenck CH, Mahowald MW, Castillo PR, Del Tredici K, Braak H: *Pathophysiology of REM sleep behaviour disorder and relevance to neurodegenerative disease.* Brain (2007); 130:2770–2788

[34] Krahn L. E., Black J. L., Silber M. H.: *Narcolepsy: new understanding of irresistible sleep.* Mayo Clin Proc (2001); 76(2):185–194